To the Graduate Council:

I am submitting herewith a thesis written by Richard D. Thoms entitled "Investigation of an Axisymmetric Missile Staging Event Using Time-Accurate and Steady-State Computational Fluid Dynamics." I have examined the final copy of this thesis for form and content and recommend that it be accepted in partial fulfillment of the requirements for the degree of Master of Science with a major in Mechanical Engineering.

Roy J. Schulz

Dr. Roy Schulz, Major Professor

We have read this thesis
and recommend its acceptance:

Edward M. Kraft

Robert T. Roach

Accepted for the Council:

C W Minkel

Associate Vice Chancellor
and Dean of The Graduate School

INVESTIGATION OF AN AXISYMMETRIC MISSILE STAGING MANEUVER USING TIME-ACCURATE AND STEADY-STATE COMPUTATIONAL FLUID DYNAMICS

A Thesis

Presented for the

Master of Science

Degree

The University of Tennessee, Knoxville

Richard D. Thoms

December, 1996

DEDICATION

This work is dedicated to my wife, Janice, and our new baby daughter, Shannon Nicole.

ACKNOWLEDGMENTS

This work was funded by the Air Force Office of Scientific Research. The funding manager was Dr. Leonidas Sakell. I would like to thank my peer review committee at AEDC for their input and advice in preparing this document. They are Dr. Robert Nichols, Fred Shope, Keith Jordan, and Robert Tramel. I especially want to thank Fred Shope for helping with the inviscid interceptor solutions, Keith Jordan for helping to teach me the general time-accurate moving mesh procedure, and Dr. Robert Nichols and Robert Tramel for the immense help provided during this work. I would also like to thank my thesis review committee for their insight and help throughout my time spent at the University of Tennessee.

ABSTRACT

Steady-state and time-accurate solutions of the Navier-Stokes equations have been obtained for the axisymmetric staging separation of a generic missile interceptor vehicle from its booster vehicle at a Mach number of 7.91. The vehicles are separated by a forward firing rocket motor located in the forward part of the booster vehicle. Hot and cold calorically perfect gas models of the separation motor exhaust jet were used for each case executed. Recommendations have been made to enhance the design process by integrating computational fluid dynamics results with wind tunnel testing for similar configurations. The dynamic effects were predicted to be large for the cases of gap/D < 0.1, and during separation motor startup. Therefore, wind tunnel testing in this region should not be solely relied upon to determine separation trajectories. Time-accurate CFD is a valuable tool for this phase of the separation maneuver and should be used to complement wind tunnel testing. It was also found that the separation rocket motor jet need not be modeled as a hot gas if gross vehicle forces are the only concern when the booster and interceptor have been separated with a gap/D greater than 0.1. If temperature sensitive instrumentation or control systems are being evaluated, hot jet modeling is required because large areas of flow separation occur on the interceptor vehicle which entrain hot gasses. Sensors in these locations could be affected.

TABLE OF CONTENTS

LIST OF TABLES

LIST OF FIGURES

NOMENCLATURE

A_{ref}	Reference area
c	Speed of sound
C_A	Axial-force coefficient, C_A = (axial force) / (qA_{ref})
D	Base diameter of interceptor vehicle and booster
gap	Axial distance between interceptor vehicle and booster
$\dot{m}$	Non-dimensional separation motor mass flux, $\dot{m}$ =(mass flux) / ($\rho_\infty c_\infty$)
M	Mach number
P	Pressure
q	Dynamic pressure
R	Perfect gas constant
Re_D	Reynolds number based on booster diameter
t	Time (seconds)
T	Temperature
U	Translational velocity
U_{dot}	Translational acceleration
X	Axial translation (+ = downstream)
Y	Distance off the body centerline
y+	Dimensionless boundary layer distance
Δt	Change in time
Δx	Change in x
γ	Ratio of specific heats (1.4)
ρ	Density
Subscripts:	
$( )_B$	Value for booster vehicle
$( )_{KV}$	Value for interceptor vehicle
$( )_t$	Stagnation condition
$( )_\infty$	Free-stream condition
$( )_1$	Condition upstream of shock
$( )_2$	Condition downstream of shock

Chapter 1

INTRODUCTION

1.1 Background

The accurate simulation of a missile staging event is of great concern to the designer of any multiple stage missile system which requires a staging maneuver. In the past, most approaches have been of the experimental "cut and try" method. There are few public or non proprietary sources that a designer can rely upon to obtain accurate information about the staging process, and the flow phenomena associated with a missile staging maneuver. The Arnold Engineering Development Center's (AEDC) Von Kármán Facility (VKF) has been a leading producer of data and knowledge for the case of hypersonic missile staging events. The techniques used at the VKF facility have yielded acceptable results, but do have several limitations. The main limitation is the inability to perform time-dependent testing. A second limitation of the wind tunnel test technique is the lack of real gas effects when simulating the separation rocket motor. The present work is intended to investigate the problems that these limitations impose on the experimental methodologies and to determine the impact of the restrictions of the techniques used in the VKF facility on test data.

The case being investigated is the staging event of a generic interceptor/booster missile at Mach 8 (7.91) flight. The interceptor is separated from the booster by means of a forward firing separation rocket motor installed in the forward part of the booster vehicle.

The wind tunnel test hardware that would simulate the staging event consists of a strut mounted interceptor vehicle and a sting mounted booster vehicle (see Figure 1). The sting has a flow-through balance through which cold high-pressure air is injected and blown through a

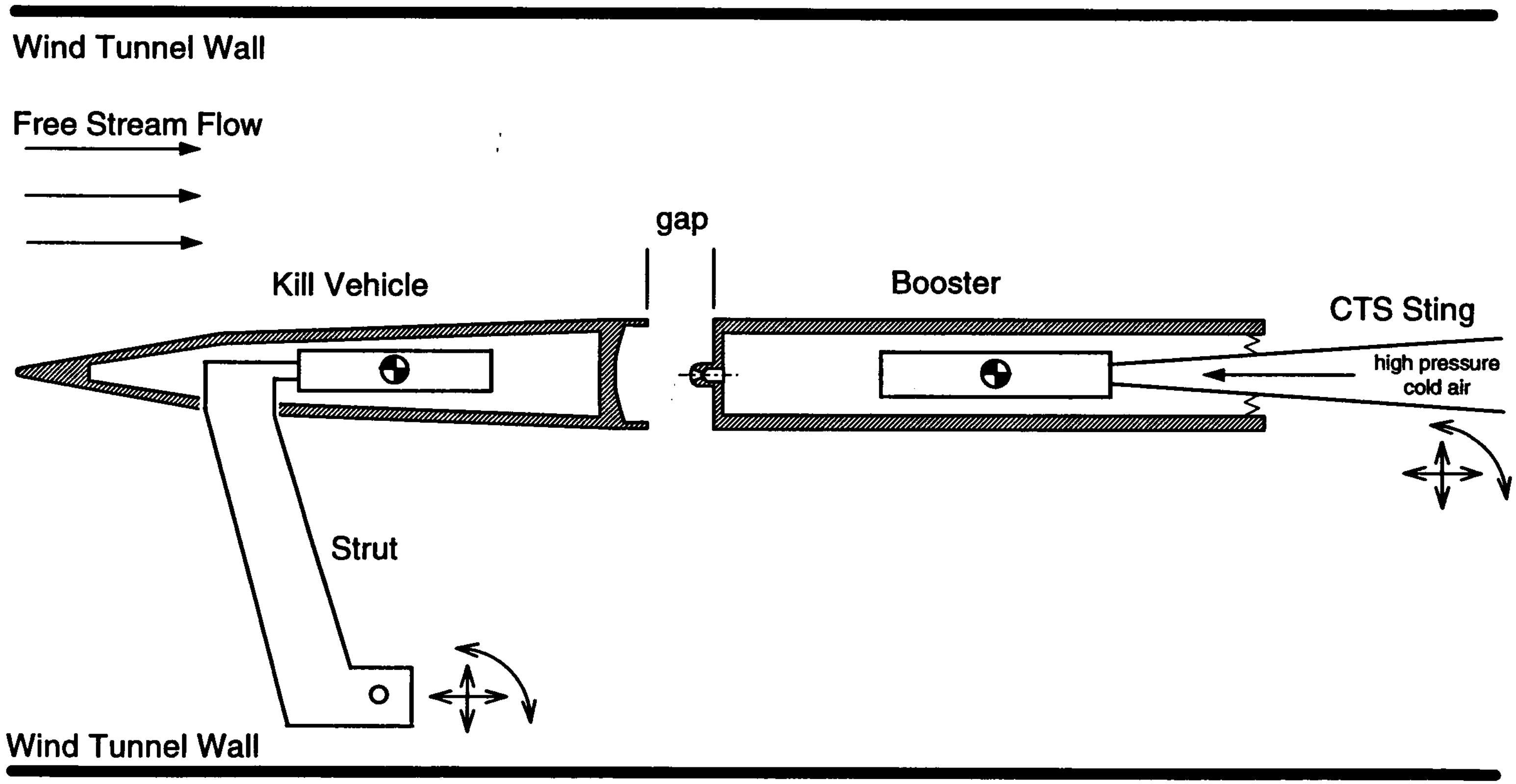

Figure 1: Typical Wind Tunnel Test Hardware

forward facing nozzle in the booster vehicle. Due to speed limitations of the model support hardware, all separation testing is done in static conditions, i.e. the booster vehicle is placed in a pre-determined position relative to the interceptor vehicle and the steady-state data are collected. The models are then repositioned electromechanically and the next data point is obtained. More detail of the wind tunnel test technique will be given in Chapter 2.

1.2 Objective of Study and Approach

There are two concerns with the static experimental technique for simulating a missile staging event: 1.) Since a staging event is a dynamic event, are there any problems associated with using steady-state data to analyze the unsteady event? 2.) Is it valid to use a cold jet to model the separation rocket motor exhaust jet? These two questions will be addressed in the present work.

A series of Computational Fluid Dynamics (CFD) solutions have been executed to help analyze the flow phenomena that are occurring in this type of stage separation event. The computational simulations are divided into two parts: 1.) Steady-state computations to closely model the wind tunnel technique. 2.) Time-accurate staging simulations to be compared to the steady-state computations to determine dynamic effects encountered during the staging maneuver. In all cases the separation rocket jet has been modeled two ways: 1.) A calorically perfect cold gas which closely simulates the conditions found in the wind tunnel technique. 2.) A calorically perfect hot gas which will can be compared to the cold gas computations to determine jet temperature effects on the staging maneuver.

The general approach of the computational experiments will be discussed in Chapter 3 and the results and analysis of the actual computational experiments are presented in Chapter 4. Conclusions and recommendations determined from these experiments are discussed in Chapter 5.

Chapter 2

EXPERIMENTAL TECHNIQUE

The experimental technique normally used in the VKF facility for this type of staging simulation makes use of the VKF Captive Trajectory System (CTS), operated in the grid mode. The CTS system is a model positioning system which is computer controlled to both position the models and perform the data acquisition, as required. The main advantage of this system is that it allows many different relative positions of the models to be tested without having to stop the wind tunnel operation and have personnel manually position the models. The grid mode refers to the mode of operation of the CTS system. In the grid mode, the CTS is used to position the models in a pre-determined set of spatial locations. The wind tunnel test technique is described in Reference 1 and can be summarized as follows:

The desired spatial locations of the model components are loaded into the CTS computer as a matrix of desired grid points; the computer then controls the static positioning of the wind tunnel model components and automatically records all the data inputs, such as wind tunnel flow conditions and model aerodynamic loads, at each spatial location or "grid point." The aerodynamic forces and moments on the CTS model (booster), including aerodynamic interference of an adjacent parent model (interceptor vehicle), are measured as a function of the relative position and orientation of the two models. This type of organized aerodynamic data, when properly processed, may be employed for body trajectory computation via any suitable trajectory program [1].

It should be emphasized that this process is a steady-state technique and thus time-varying or dynamic effects are not measured. The wind tunnel technique simply measures steady-state loads with the vehicles in various relative positions. A major disadvantage of the wind tunnel technique is that no separation motor start-up effects can be simulated. The VKF high pressure air system is used to supply cold high pressure air through a special flow-through balance system and into the separation motor nozzle plenum chamber. The use of cold air (T_t - 350°R) in the wind tunnel technique is a concern when the real separation rocket exhaust has stagnation temperatures greater than 1700°R. Also, the uncertainties in the measured model position of 0.20 inches (full scale) [1] are relatively large when placement of the vehicles within 0.10 inches (full scale) has been found to be critical.

Chapter 3

COMPUTATIONAL TECHNIQUE

There are two computational techniques that are used in this work. The first is a computational simulation of the steady-state experimental technique described in Chapter 2. The second technique determines the separation trajectory using time-accurate CFD to determine flow about the bodies and a six-degree-of-freedom integrator to determine the body position. Upon analyzing and comparing the results from these two techniques, the dynamic effects during separation will become apparent, and it will then be possible to determine if the experimental steady-state technique is valid for this type of missile staging maneuver.

For both of these techniques, the temperature of the separation motor will be modeled in two ways. The first is as a cold jet of perfect gas to simulate the experimental technique, and the second is as a hot jet of perfect gas to more closely model the effects of separation motor exhaust gas temperature on the separation maneuver. Comparing hot jet and cold jet simulations will help to determine if the experimental technique results are jeopardized by the cold jet assumption.

For all of the cases discussed the same assumptions apply. The separation rocket jet is modeled as a perfect gas with a ratio of specific heats equal to 1.4. No attempt was made to model combustion products or chemical reactions for the jet or the bulk flow around the vehicles. The vehicles are modeled as axisymmetric rigid geometries and thus only axial displacement is allowed during the trajectory simulation. The wall boundary conditions assumed are those due to laminar, adiabatic boundary layers.

3.1 Steady-State Baseline Technique

The intent of the steady-state baseline technique is to numerically simulate or predict the experimental results that occur in the VKF CTS tests. The baseline technique is a steady-state solution of the flow field with the bodies in static positions and with the separation motor flow fully developed. The results from these static solutions will be compared to the dynamic solutions to determine the dynamic effects encountered during a staging simulation.

There are two major steps to obtaining the baseline solutions. The first is the construction of a multi-mesh computational mesh system, with intermesh communications. The second is the execution and analysis of the flow solutions.

3.1.1 Construction of the Computational Mesh System

An important consideration during the mesh generation process is the need to use the same meshes for both the baseline and staging simulations. If the same meshes are used in both simulations then any differences found during analysis will not be the result of the computational meshes used. There are several types of mesh systems that could be used for a moving-body time-accurate CFD solution, unstructured, blocked, and overset. The requirement for viscous modeling all but rules out the use of an unstructured mesh system at this time. There are two choices available for structured meshes; blocked or overset. There has been some prior work [2] done with blocked meshes but it is felt that this approach is not general enough for full 3-D motion which is a future direction of this work. The chimera system [3-7] is used in the present study because mesh generation is relatively simple and regeneration of the meshes is not necessary to perform the rigid body movement.

The basic chimera overset-mesh procedure allows for the generation of a system of relatively simple, overlapping meshes, each describing a subdomain of a complex aerodynamic configuration. Interpolation coefficients determine boundary conditions at overlap boundaries for each mesh from the interiors of neighboring meshes. Body movement is performed by translating and rotating the meshes that define the body geometry and updating the interpolation coefficients. This method has been used with success on several time-dependent store separation cases [8,9].

The PEGSUS code [10] is used in this study to determine the interpolation coefficients that allow communication of flow information between the subdomains. The code performs two functions. The first function is the removal of points from other subdomains that lie within the solid surface of the geometry being considered. This first step is called hole creation. The second function is the generation of trilinear interpolation coefficients to provide information to boundary points. The boundaries that require this information include overlapping computational surfaces and boundaries that are created during the hole creation process.

3.1.2 Steady-State Solution

The flow solver used in this study is the AEDC developed XAIR which is a chimera implementation of a three-dimensional implicit algorithm used to approximate the solution of the Navier-Stokes equations for a calorically perfect gas [5,7]. The implicit, approximate-factorization scheme employed was developed and first applied to flow problems by Beam and Warming [11]. The coded form of the scheme is a vectorized enhancement of the version developed by Steger and Pulliam [12]. The chimera overset implementation was developed by Steger, Benek, Dougherty, and Buning [4,6,7]. The second- and fourth-order implicit and explicit smoothers of Benek, et al [13] were used to suppress oscillations and improve stability of the central-difference algorithm. The algorithm is second-order accurate in space and first-order accurate in time. Boundary conditions are set explicitly.

All of the solutions for the steady-state baseline technique modeled the rocket motor flow as well as the flow over the vehicles. To obtain a steady-state solution, the flow solver is executed until the force and moment coefficients are converged to four significant digits.

3.2 Dynamic Staging Technique

There are three main steps to the present CFD dynamic staging technique: construction of the CFD mesh system, calculation of the steady-state initial condition solution, and the prediction of the trajectory. The mesh construction process has been described in Section 3.1.1. Described below and illustrated in flow chart form in Figure 2 is the initial condition and time-accurate trajectory prediction process.

3.2.1 Initial Condition Generation

This solution is executed as described in Section 3.1.2 for the static solutions with the exception that the separation rocket motor is not operating. To observe the effects caused by motor startup the initial condition must be obtained with the separation rocket motor off. Because there is almost no flow in the interstitial region the flow-field becomes incompressible (i.e. density does not change with time). When the Mach number approaches zero, the compressible forms of the Navier-Stokes equations become stiff because the eigenvalues are widely separated. This stiffness slows the convergence of the solution tremendously. To overcome this problem the flow solver is executed until the outer flow-field surrounding the model has converged. Then the interstitial region is filled with flow values taken from just upstream of the gap on the wall of the interceptor vehicle. This ensures that the flow values are consistent with the conditions in the boundary layer, and since the values are taken at the wall, all velocities are

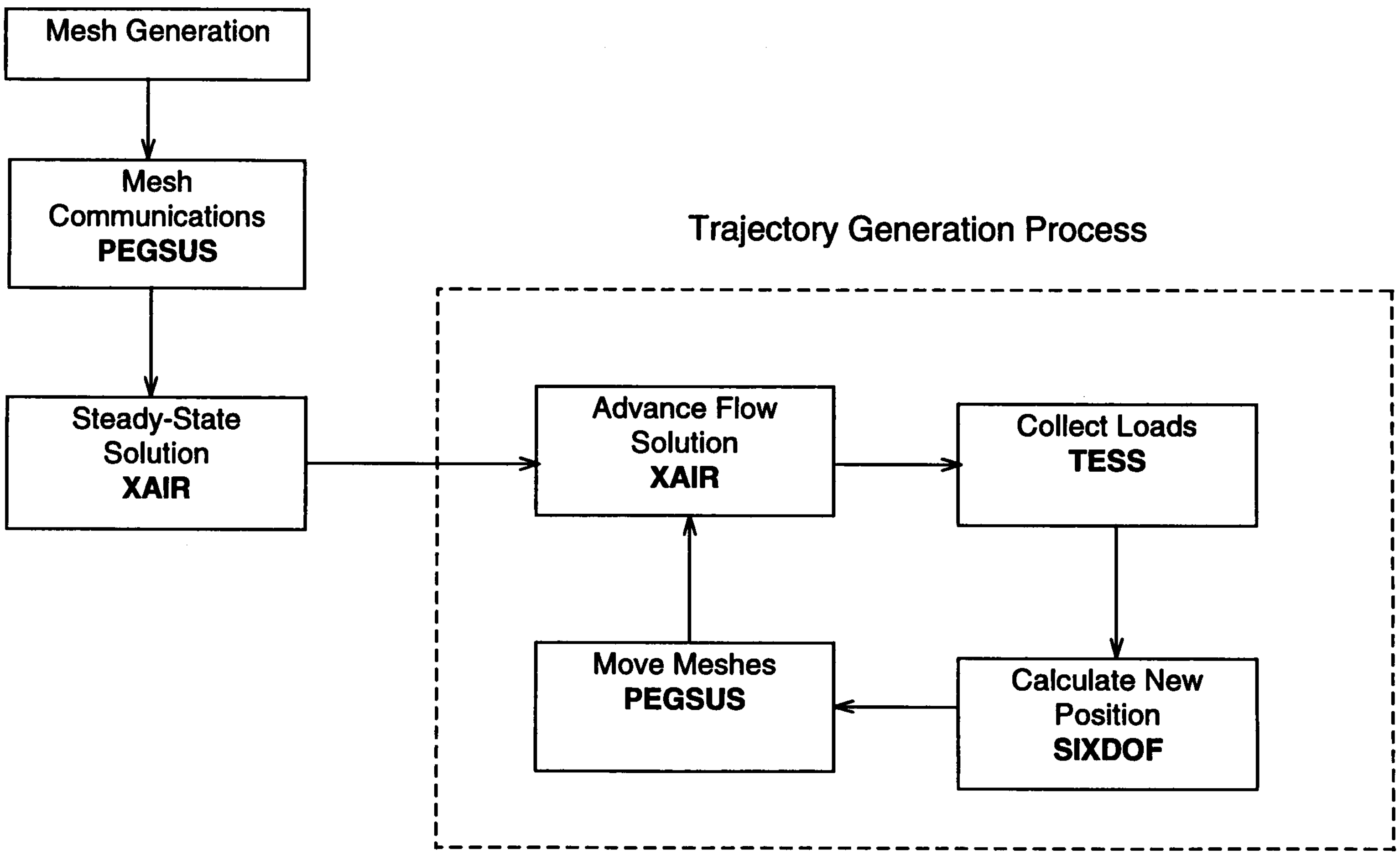

Figure 2: Computational Process Flow Chart

zero. After this modification to the interstitial flow-field region, the solution is executed until the force and moment coefficients have converged to four significant digits.

3.2.2 Time-Accurate Trajectory Prediction Process

The trajectory prediction process was developed at AEDC [9] and is actually a loop of four sub-steps which are discussed in turn. After a steady-state solution is obtained as an initial condition, execution of the set of programs occurs serially during each time step as the prediction marches forward in time. The time-accurate trajectory prediction process begins with the flow solver advancing, in a time-accurate manner, one time step to determine a new flow-field solution. Next the pressure and viscous stresses computed at the surface of the body are integrated over the surface area to determine the aerodynamic force and moment coefficients. Using these coefficients the equations of motion of the bodies are integrated over the time step to determine the next position of each body. Finally, the moving meshes representing the bodies and flow-fields together are repositioned within the mesh system and returned to the flow solver to begin the next time step.

3.2.2.1 Flow Solution

The first substep advances the flow solution one time increment in a time-accurate manner. The flow solver is the same as that used to obtain a steady-state solution, XAIR. The solution differs from the steady-state in that time metrics are included, and a moving wall boundary condition is used on solid surfaces which are in motion. The separation rocket motor exhaust flow is controlled by specifying the inlet total pressure and total temperature. A Newton's iteration method is used to ensure that the mass flow at the nozzle inlet is consistent with the mass flow at the nozzle throat.

3.2.2.2 Force and Moment Integration

The calculation of forces and moments requires the integration of pressures over the surface area of the configuration. Allowing meshes to overlap means that some regions on a surface will be defined by more than one mesh, and the area over which integration is to be performed will be multiply defined. The problem is exacerbated in many overset mesh applications because the regions that are multiply defined are often those which experience the most complex flow. As a result small errors in defining areas in complex flow regions can result in large errors in calculated forces and moments.

The TESS code [14] is an interactive program which contains various routines that allow the development of a singly defined surface from a system of structured overset meshes. The approach is to develop a surface definition of a complex configuration using triangular elements that incorporate all of the surface points contained in the overlapping structured meshes. All surface points are retained, and any number of overlapping surfaces can be accommodated. The code also provides routines for integrating pressure and viscous stresses over the resulting singly defined surface.

3.2.2.3 Six-Degree-of-Freedom Integration

The SIXDOF code [9] uses the aerodynamic force and moment coefficients acting on the body and the physical information about the body (such as mass and reference area) to calculate the next position and orientation of the body. SIXDOF assumes that all bodies are rigid. The output from SIXDOF includes time histories of the motion that includes the translation, rotation, velocities, and accelerations of reference points.

3.2.2.4 Mesh Movement / Communications

Once the new position of the body has been calculated, the computational meshes that model the body are translated and rotated to the new position. Interpolation coefficients are updated for all overset boundaries requiring flow-field information from another mesh. After this step has been performed the meshes are passed back to the flow solver to begin again the process of flow-field calculation. In this manner the trajectory prediction of the interceptor-booster pair is carried out as long as necessary.

Chapter 4

RESULTS AND ANALYSIS

Details of the simulations and the results obtained are presented in this chapter. Some validation and analysis of these results, with respect to the ultimate goal of this work, are also discussed.

4.1 Computational Mesh System

The test models simulate an axisymmetric generic missile interceptor / booster configuration. The interceptor vehicle is a hemisphere bi-conic cylinder. The booster is a cylinder with a flat forward face that contains the separation rocket motor. A drawing of the test articles is presented in Figure 3.

An overall view of the mesh system and an enlargement of the mesh system in the interstitial region is given in Figure 4.The vehicles and flow field surrounding them are modeled by a total of eight meshes with the names and computational mesh dimensions given in Table 1 . The same computational meshes were used for all of the results discussed below. The computational volume is an axisymmetric wedge or azimuthal sector spanning 2°, and is three computational planes wide. The off-wall mesh spacing maintains a y+ value of approximately 10.

The PEGSUS code [10] is used to provide all of the interpolation coefficients and to perform hole cutting in the interstitial region as the gap is changed. The "double fringe" option of PEGSUS is used to provide two layers of interpolation cells at each chimera overlap boundary. This allows the fourth-order smoothing to be maintained at overlap boundaries. The mesh

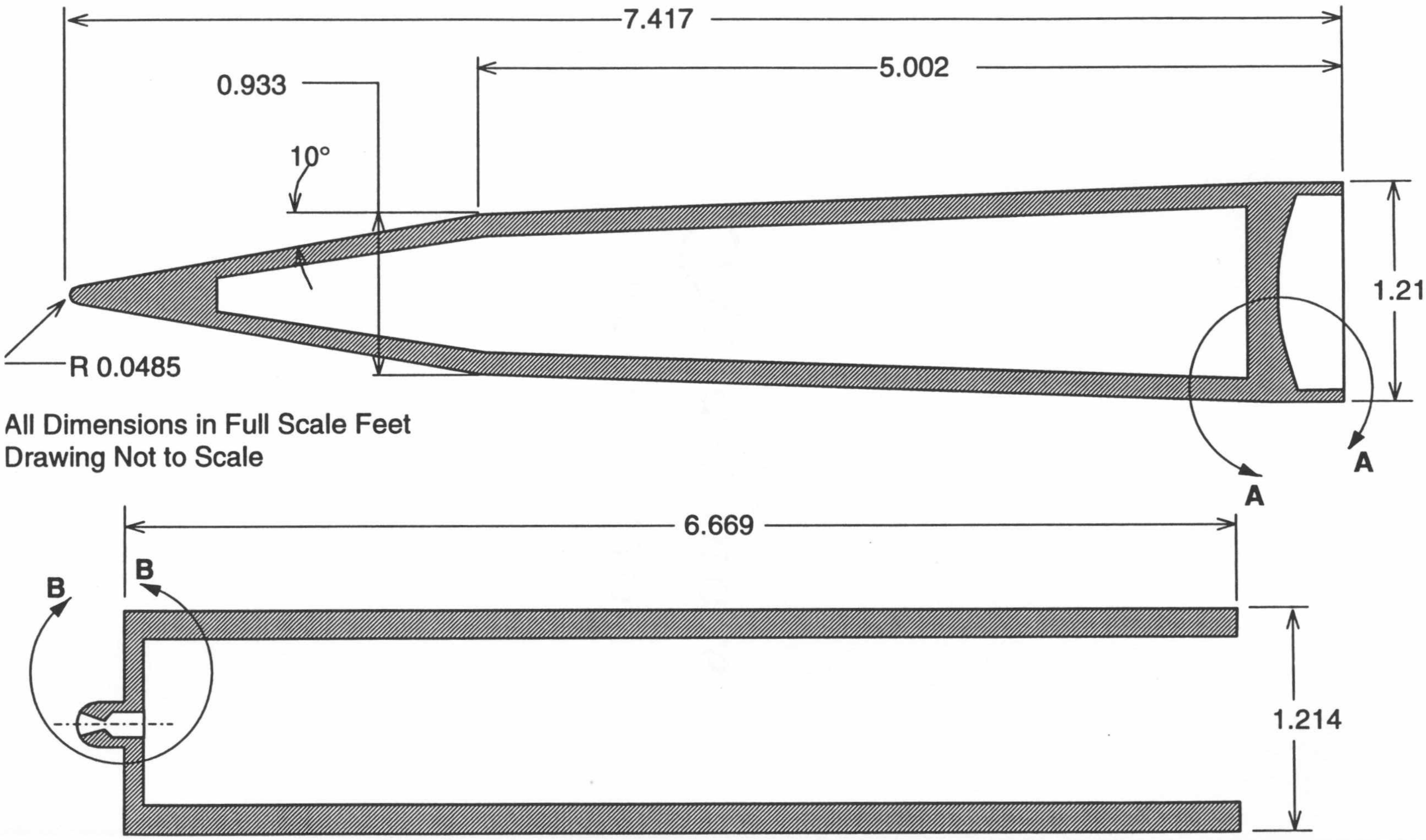

Figure 3: Test Article Geometry

All Dimensions in Full Scale Feet
Drawing Not to Scale

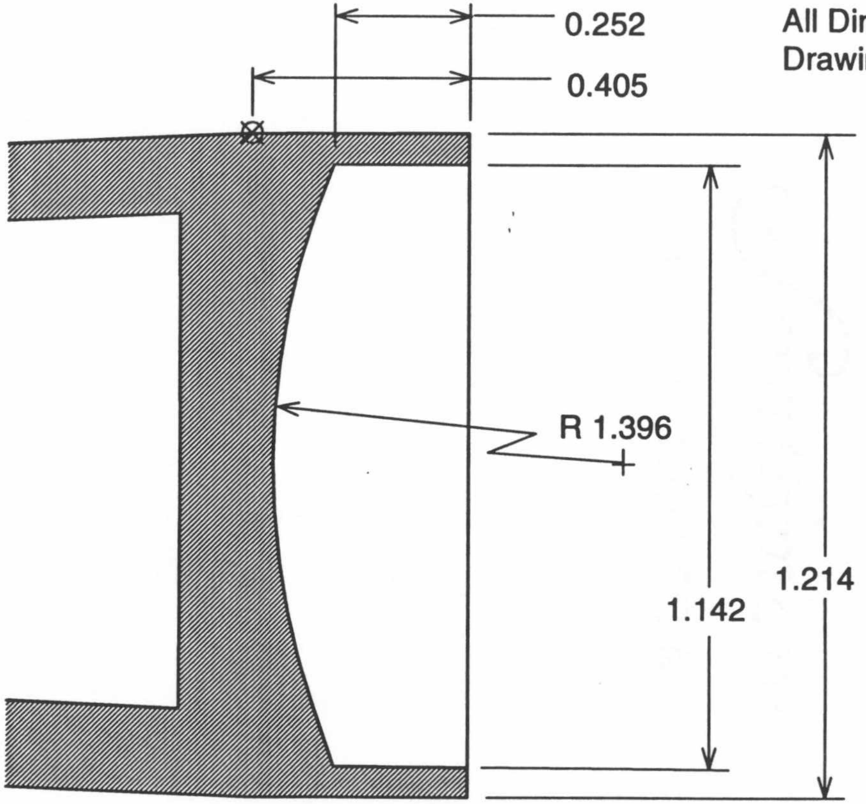

DETAIL A

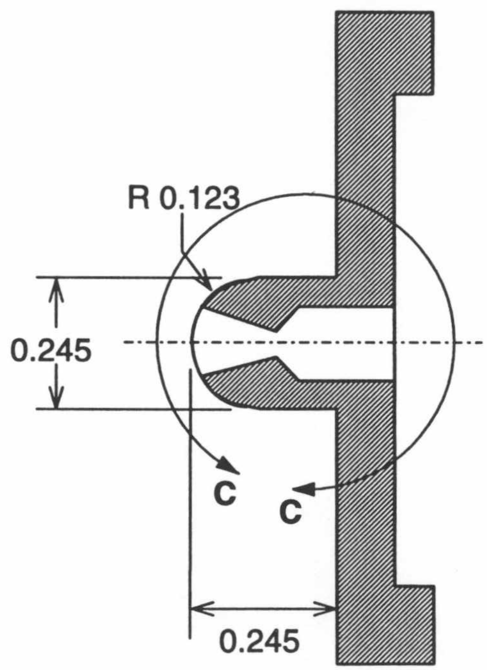

DETAIL B

Figure 3 (continued)

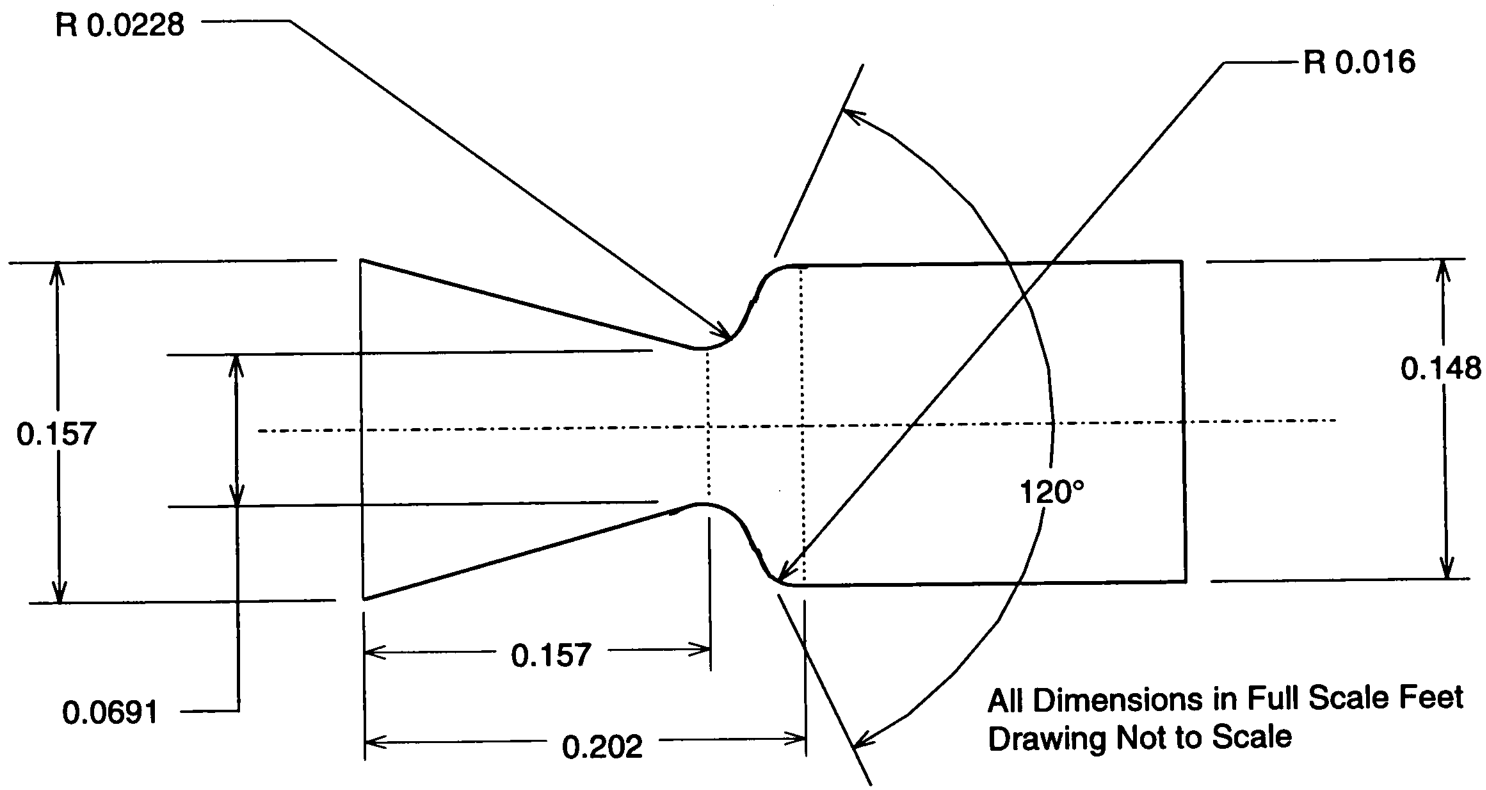

DETAIL C

Figure 3 (continued)

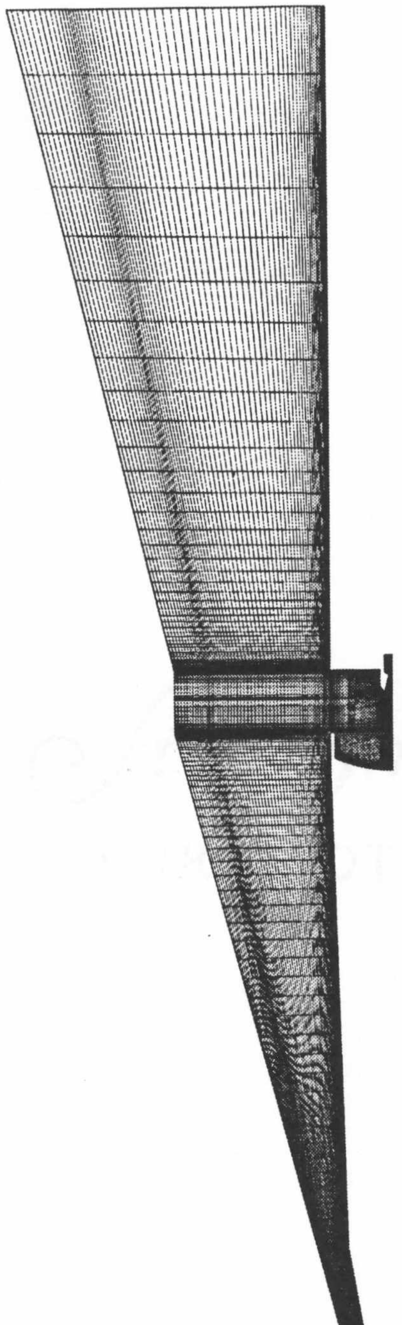

Figure 4: Computational Mesh System

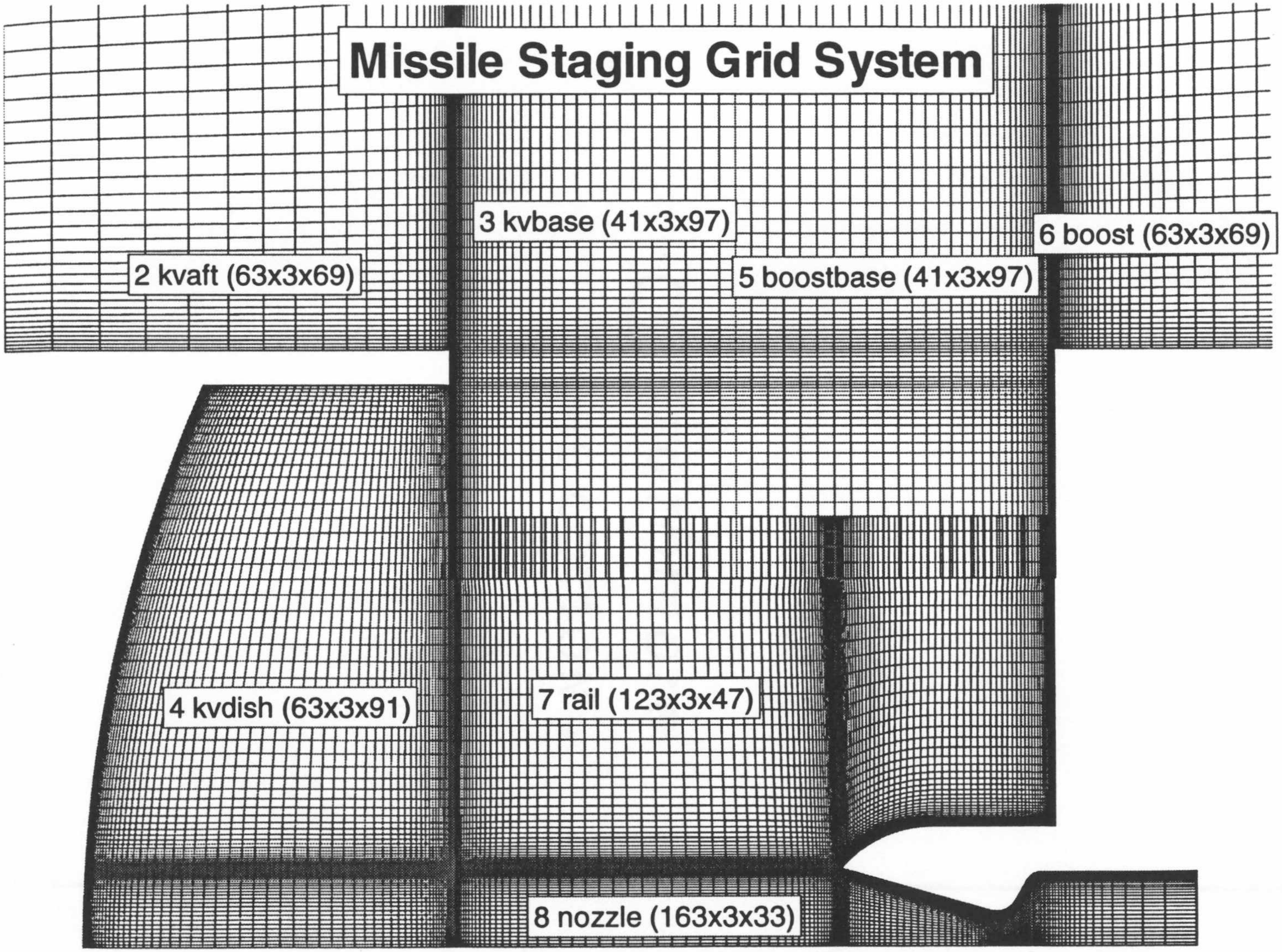

Figure 4 (continued)

Table 1: Computational Mesh Names and Dimensions.

Mesh	Name	Dimensions
1	kvfore	63 x 3 x 69
2	kvaft	63 x 3 x 69
3	kvbase	41 x 3 x 97
4	kvdish	63 x 3 x 91
5	boostbase	41 x 3 x 97
6	boost	63 x 3 x 69
7	rail	123 x 3 x 47
8	nozzle	163 x 3 x 33

system is constructed in such a way as to maintain point to point co-location at mesh overset boundaries as much as possible. This method reduces the chance of any interpolation errors becoming present in the solutions because the cells are co-located and therefore the interpolation coefficients are either one or zero (i.e. flow values are directly transferred from one mesh to another without interpolation).

4.2 Steady-State Baseline Results

A total of eight steady-state solutions have been completed. The flow conditions are given in Tables 2 and 3 and the axial-force coefficients determined by the solution are given in Table 4. The solutions are a matrix of two jet temperatures and four axial positions (gap/D = 0.0075, 0.0170, 0.2500, and 0.5000). The free-stream conditions are representative of those that would be found in the Von Kármán Facility (VKF) wind tunnel 'B' and are given in Table 2. In order to take advantage of the axisymmetric geometry, the angle of attack is 0° in all cases. The chamber conditions of the two jets are given in Table 3. Recall that the cold jet case simulates the typical conditions that would be available in the wind tunnel using the high pressure

Table 2: Free-stream Conditions for Steady-state Solutions.

Variable	Value	Unit
M_∞	7.91	-
U_∞	3679	ft/sec
ρ_∞	1.2795x10-5	slug/ft^3
$Re_{D\infty}$	3.04 x 106	-
P_∞	0.0137	psia
T_∞	90.1	°R

Table 3: Chamber Conditions for Separation Rocket Motor.

Variable	Hot Jet Case	Cold Jet Case
P_t/P_∞	3622.	3650.
T_t/T_∞	19.03	3.613

Table 4: Steady-State Axial-Force Coefficients

Gap/D	Hot Jet Case		Cold Jet Case	
	Booster	Interceptor	Booster	Interceptor
0.0075	34.40	-34.37	35.53	-35.52
0.0170	8.583	-8.467	8.463	-8.307
0.2500	1.602	-1.484	1.568	-1.478
0.5000	1.312	-1.236	1.300	-1.360

cold air injection system to simulate the separation rocket motor exhaust jet. The hot jet case more closely models the temperature of an actual separation rocket motor.

The solutions were executed until the axial-force coefficients had converged to four significant digits. However, in the cases of the gap/D = 0.25 and 0.50, the solutions did not reach a steady-state but the axial-force coefficients oscillated with a small amplitude about a mean value. The mean value of the axial-force coefficients are what will be considered the converged coefficients for these cases. Given in Table 4 and Figure 5 are the steady-state axial-force coefficients obtained with these solutions. For the interceptor vehicle, the axial-force coefficient is obtained by integrating the forces over all of the solid surfaces. For the booster, the forces are integrated over all of the solid surfaces and the separation motor plenum inlet plane. The force applied due to momentum of the fluid flow through the plenum inlet plane is then calculated and added. Since the booster base is not modeled, a pressure equal to P_∞ is applied evenly across the base.

Upon analyzing Figure 5 it becomes apparent that the bulk of the forces acting on the vehicles is generated by the relatively high pressure in the interstitial region. This is illustrated by the fact that the booster and interceptor vehicle axial-force coefficients are of the same magnitude but different signs, even considering forebody drag and afterbody base pressure effects. Also apparent are the extremely high forces encountered when the vehicles are placed with the smallest gap distance between them. This is due to the high pressures in the interstitial region.

The only difference in axial-force between the hot jet cases and the cold jet cases is for the position of gap/D = 0.0075. In this case the difference between the hot jet and cold jet axial-force is less than five percent.

Figures 6-9 illustrate constant Mach number and constant normalized temperature profiles for different gap/D values. The figures show the entire flow field as well as an enlargement of the interstitial region. Shown in the top half of each figure is the hot jet solution while the bottom half of each figure shows the cold jet solution.

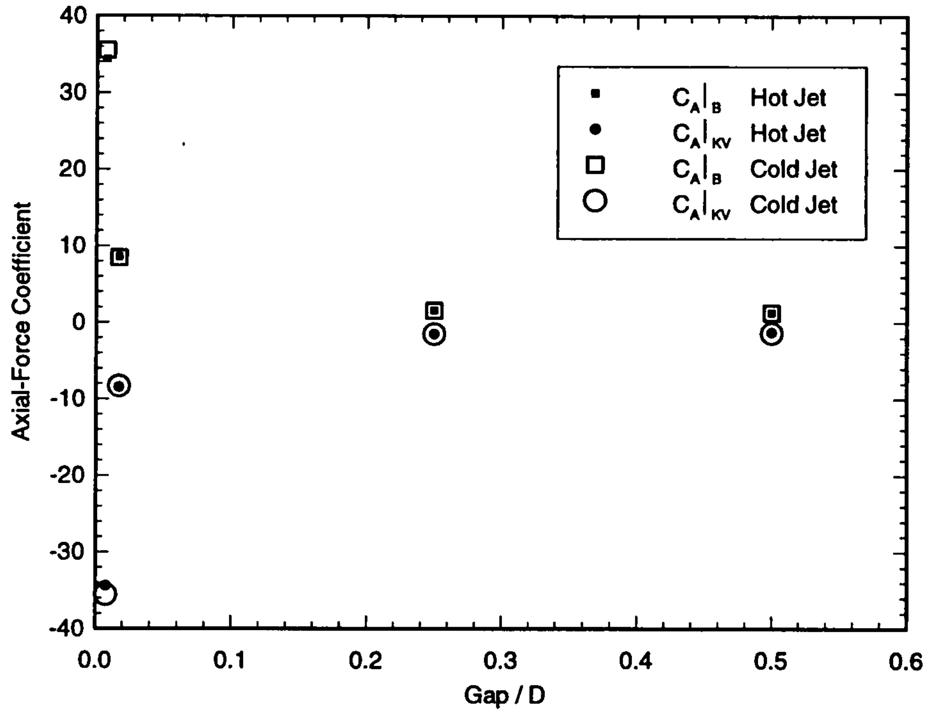

Figure 5: Steady-State Axial-Force Coefficient versus Gap/D

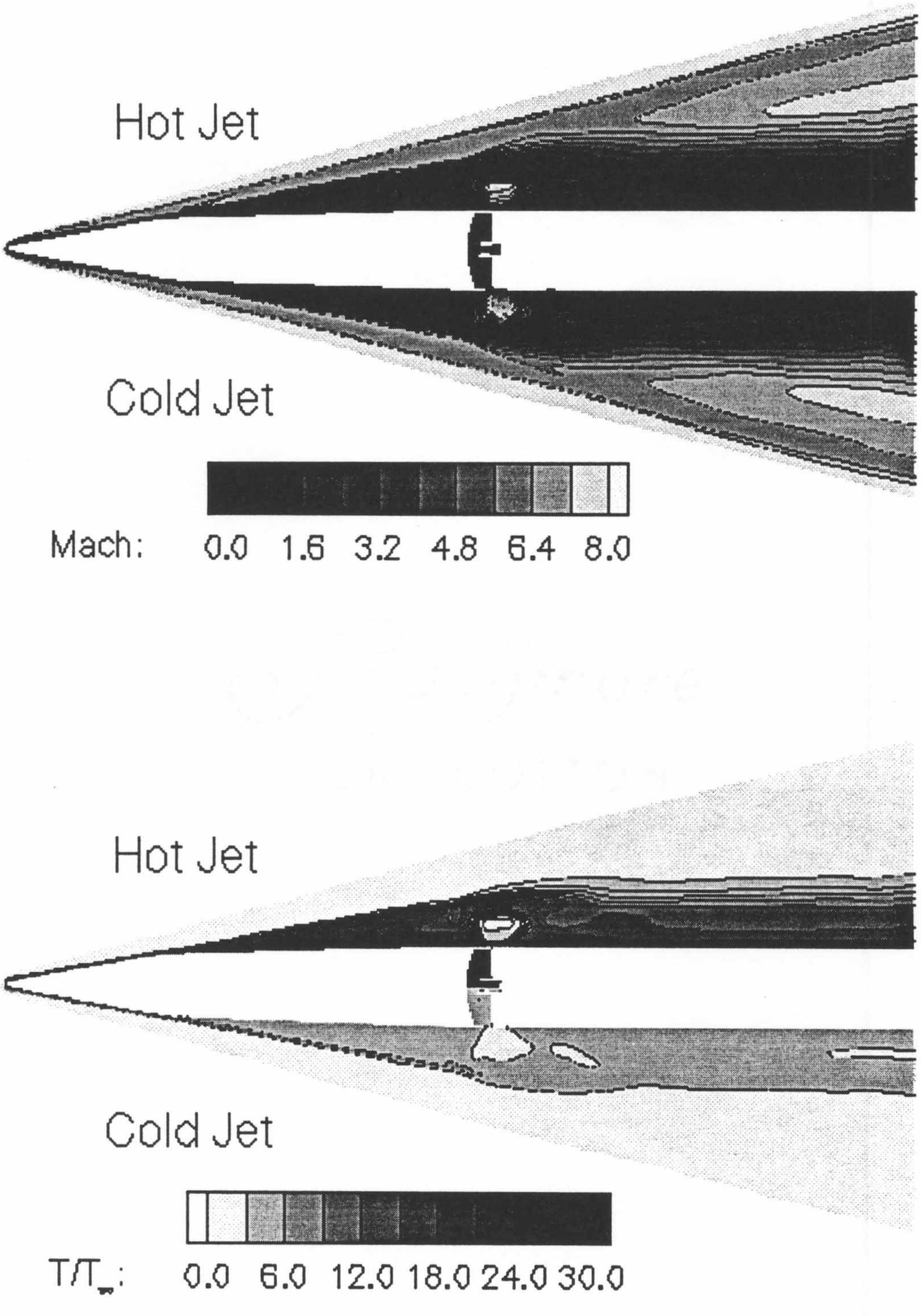

Figure 6: Mach Number and Normalized Temperature Distribution for Static Case Gap/D = 0.0075 (hot jet and cold jet)

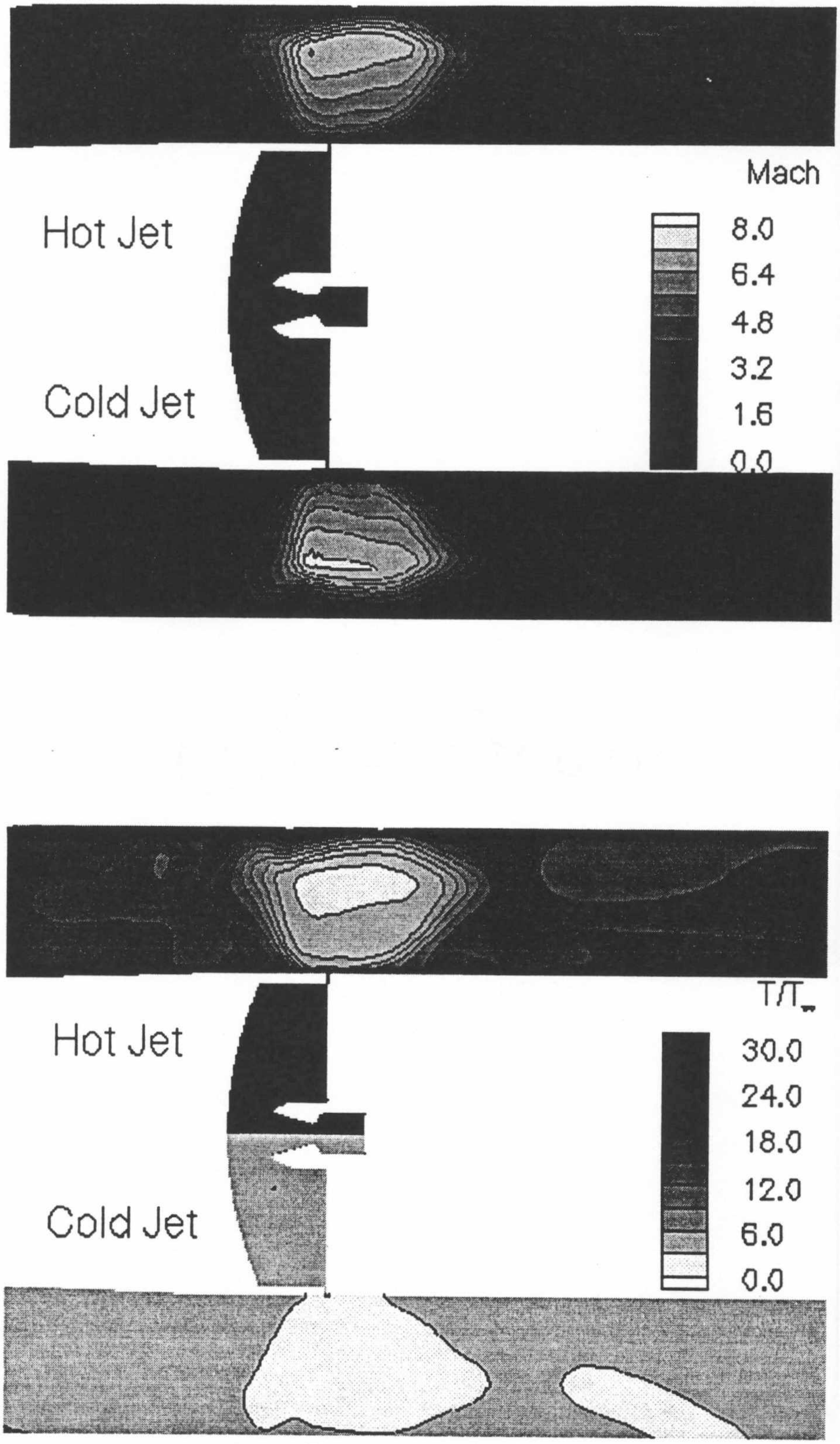

Figure 6 (continued)

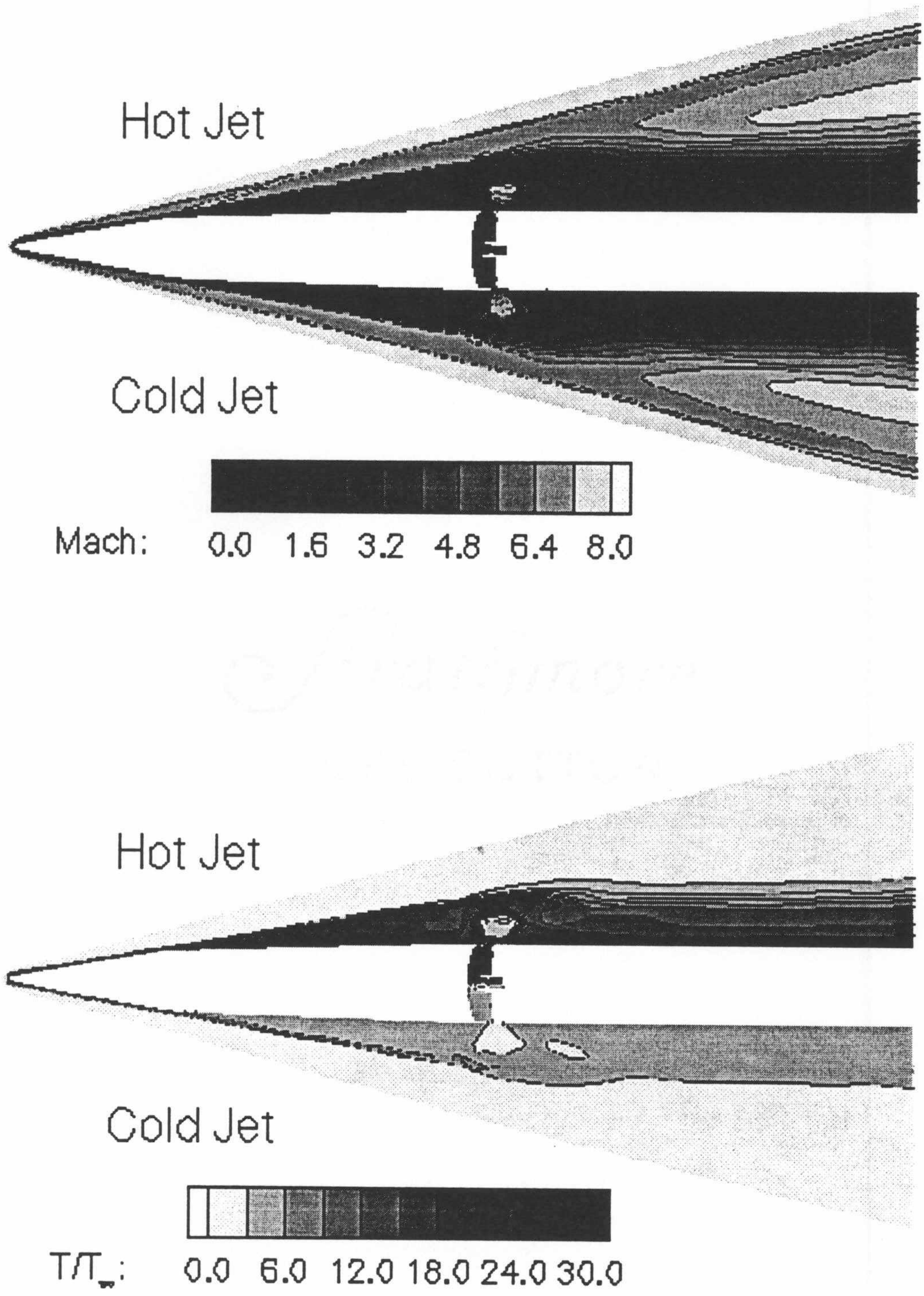

Figure 7: Mach Number and Normalized Temperature Distribution for Static Case Gap/D = 0.0170 (hot jet and cold jet)

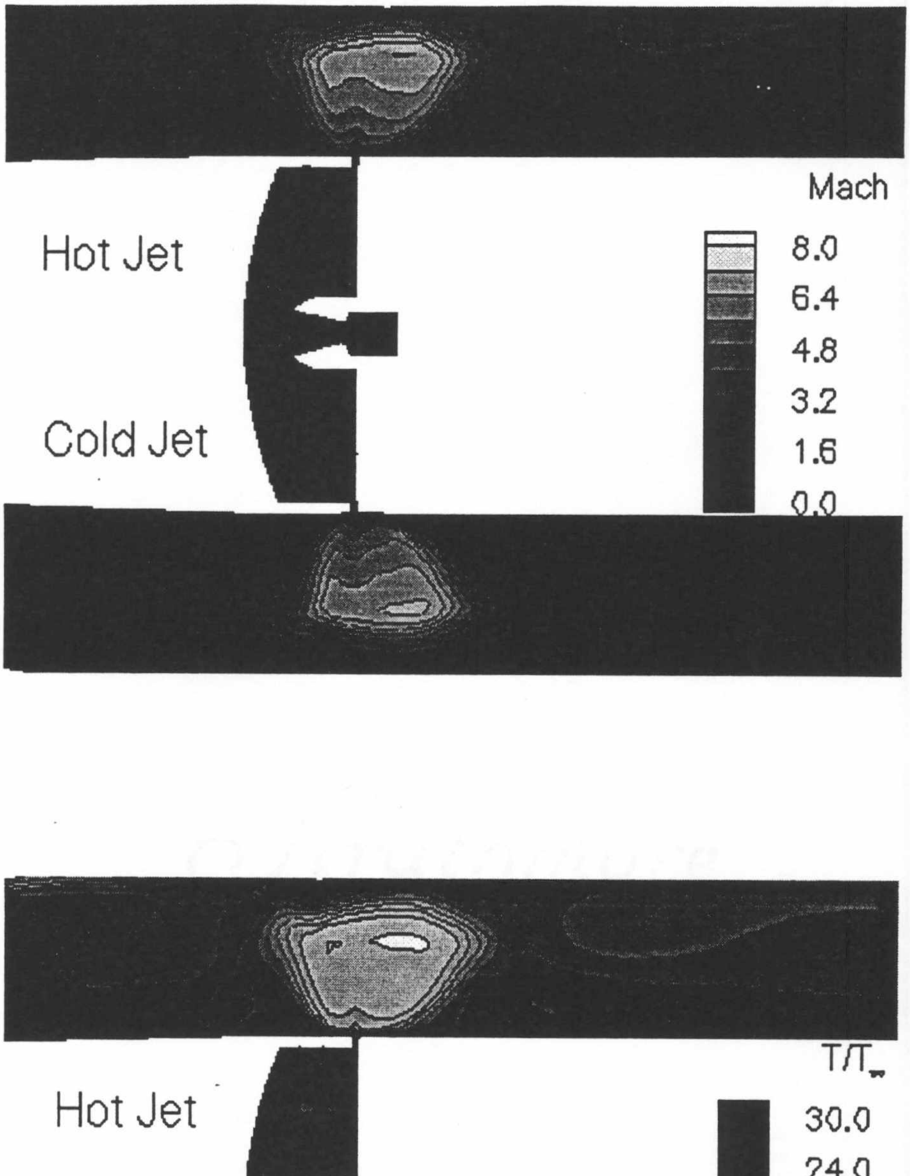

Figure 7 (continued)

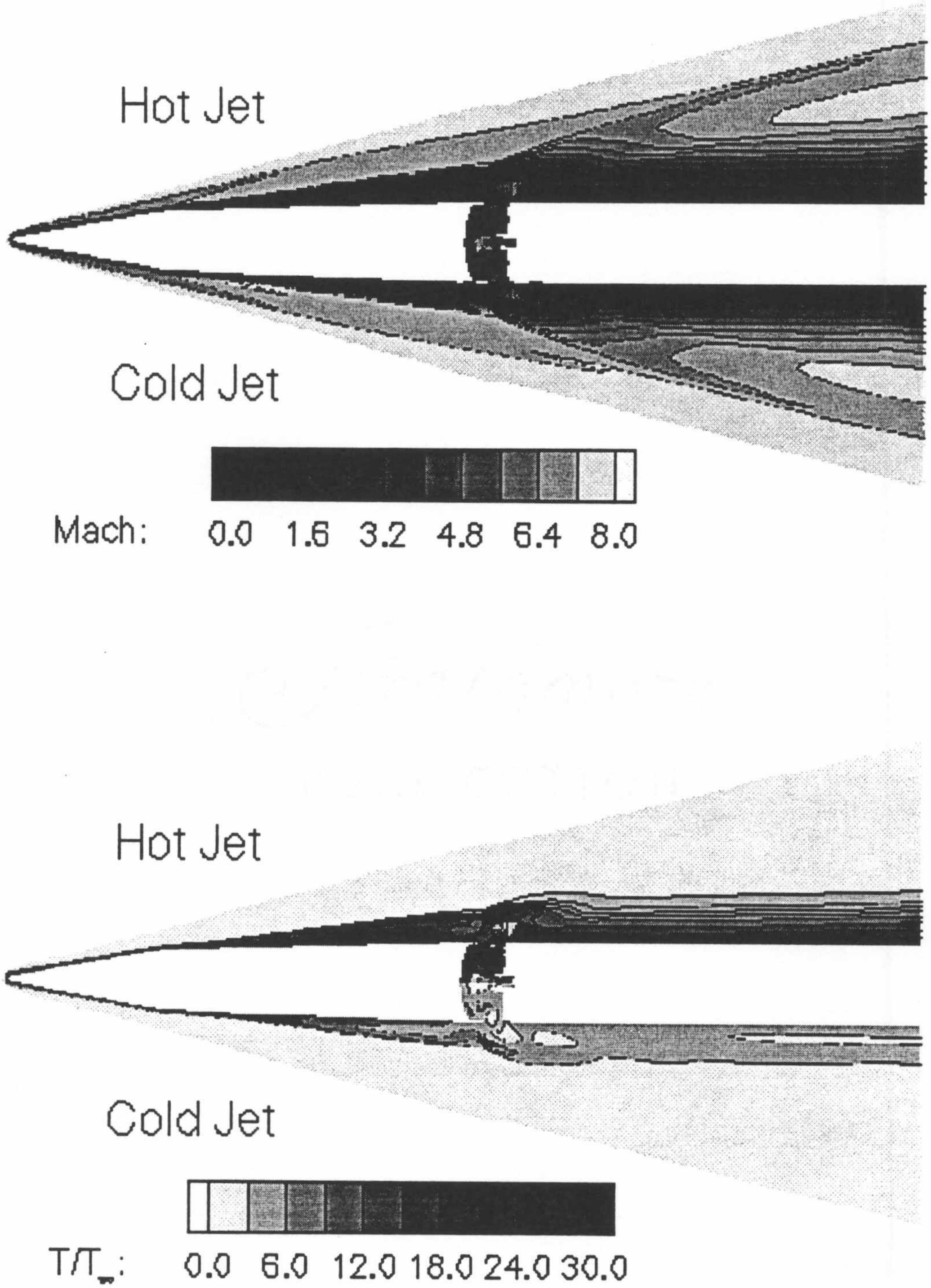

Figure 8: Mach Number and Normalized Temperature Distribution for Static Case Gap/D = 0.2500 (hot jet and cold jet)

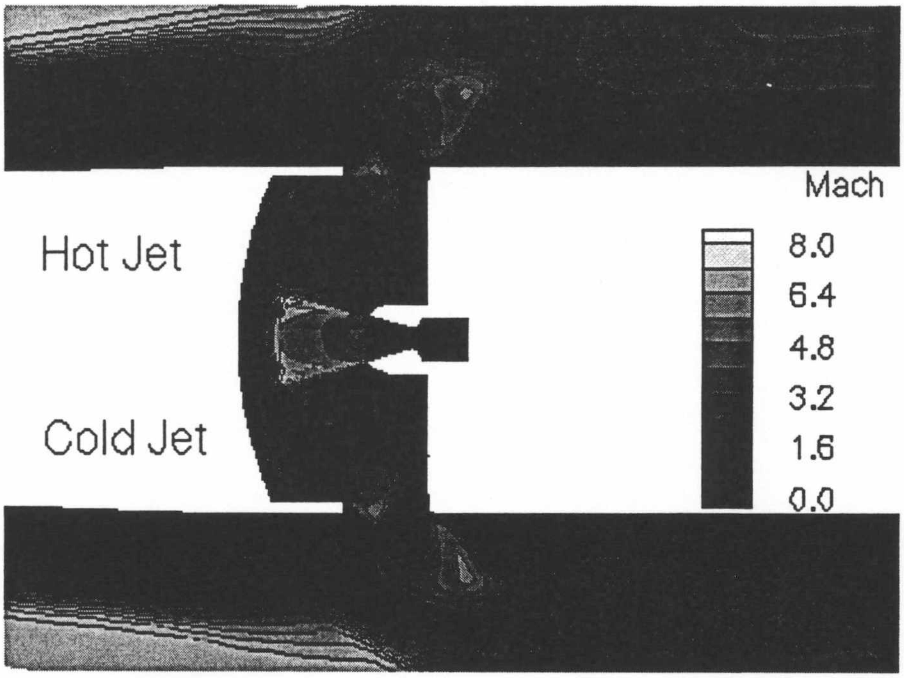

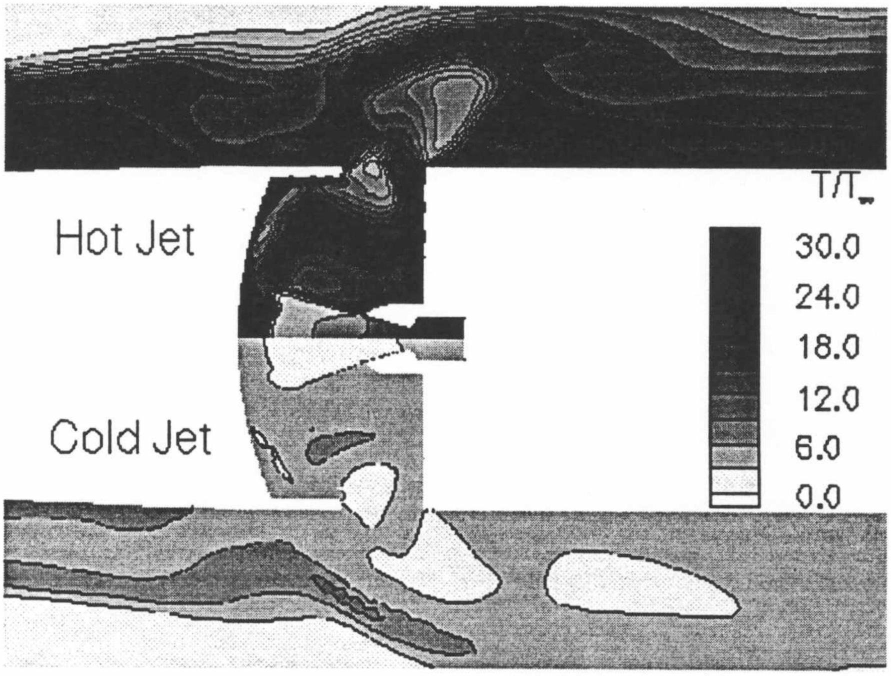

Figure 8: (continued)

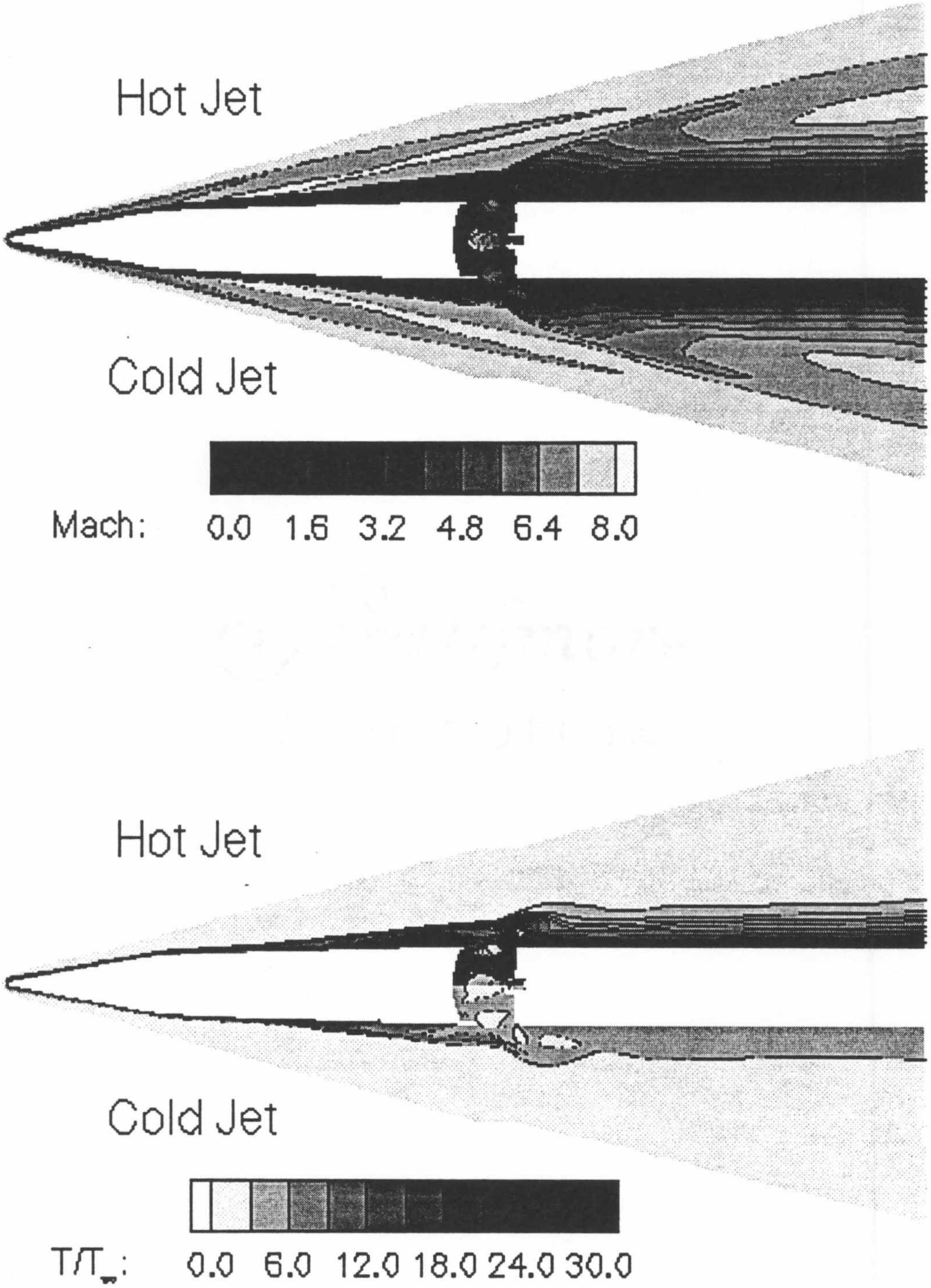

Figure 9: Mach Number and Normalized Temperature Distribution for Static Case Gap/D = 0.5000 (hot jet and cold jet)

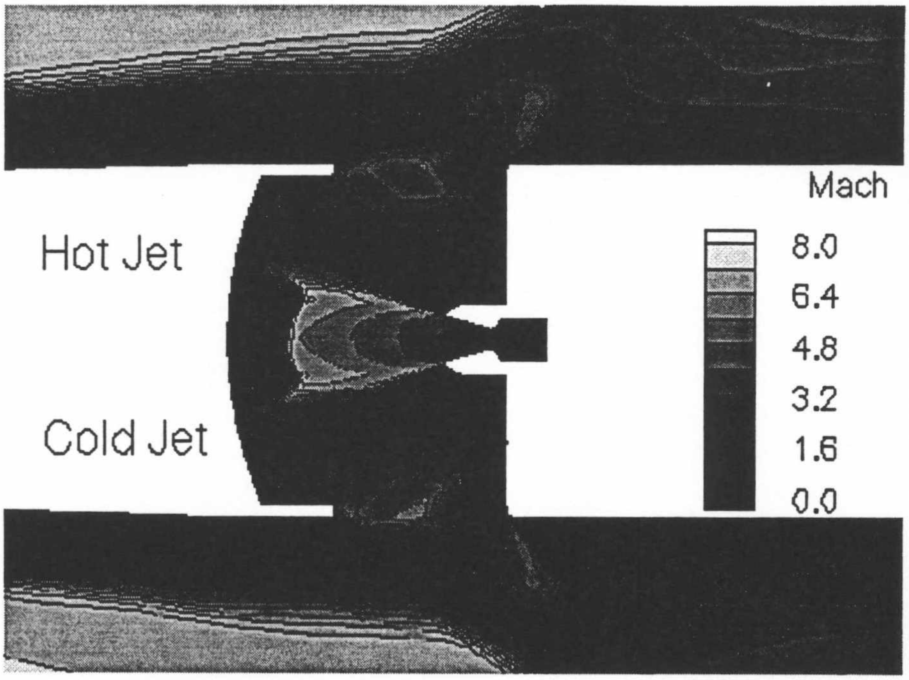

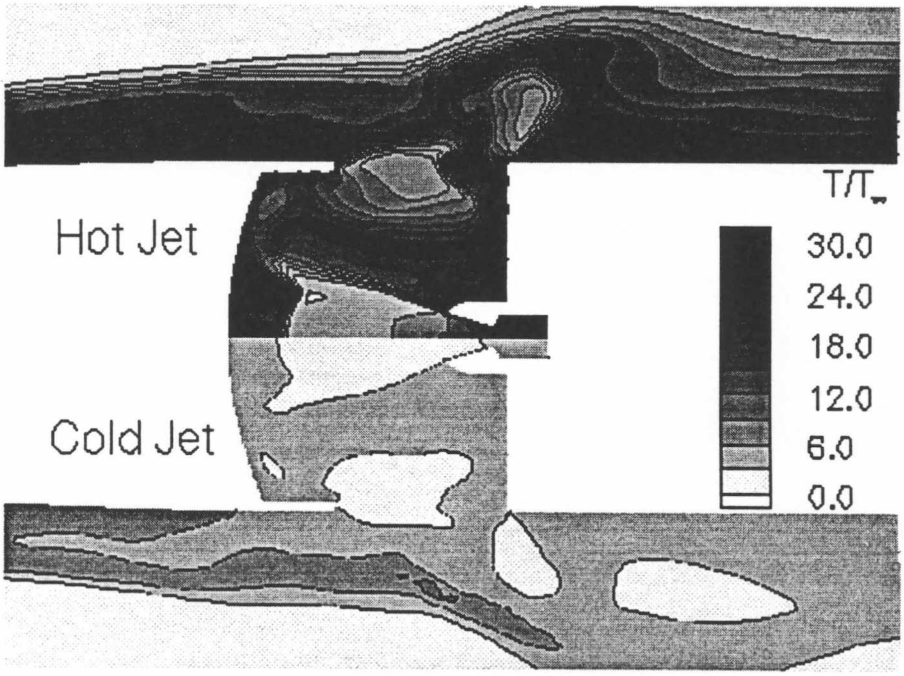

Figure 9 (continued)

One phenomena that is present in all cases is the separation of flow caused by the circumferential jet emerging from the gap between the two vehicles. This separation migrates upstream on the interceptor vehicle as the jet develops. The separation is stopped by the cone junction due to the higher momentum flow that is present just upstream of the cone junction. This separated region may be of interest to a missile designer since the separation and high temperature gases migrating upstream could affect jet interaction control systems and seeker function.

As the gap/D becomes larger more flow is entrained into the gap region. This is shown in Figures 8 and 9 as a strong recirculation in the interstitial region. In fact there are at least two counter rotating regions visible and upon closer examination more rotating regions can be found.

The temperature of the separation rocket motor has little effect on the Mach number but obviously has a large effect on the temperature of the flow-field. It is clear that the separated flow on the interceptor provides a path for hot gases from the rocket motor to migrate upstream. Also there are stagnation areas on the booster face, namely the corner between the booster face and outer geometry of the nozzle, that reach very high temperatures. Both of these temperature effects may be of concern to a designer.

An interesting item to note about these steady-state calculations is that the mass flow of the nozzle is relatively constant throughout the ranges of gap/D for a given jet temperature. This indicates that the nozzle was always choked for each of these cases. Tabulated values of nozzle mass flow calculated from the solution at the nozzle throat vs. gap/D are given in Table 5. Even though the nozzle is always choked, it is important to model the entire nozzle downstream of the throat, as can be seen by investigating Figures 6 and 7. For the case of gap/D=0.0075 the flow is separated from the nozzle exit up to the throat of the nozzle.

Table 5: Steady-State Separation Rocket Motor Mass Flux.

Gap/D	Hot Jet	Cold Jet
0.0075	526.7	1218.
0.0170	526.7	1218.
0.2500	526.4	1219.
0.5000	526.7	1218.

As a side analysis the mass flux at the throat was determined using isentropic relations to check the validity of the present calculations. The equation for this is given below:

$$\dot{m} = \frac{P_t}{\rho_\infty c_\infty}\sqrt{\frac{\gamma}{RT_t}}\left(1+\frac{\gamma-1}{2}\right)^{-\frac{(\gamma+1)}{2(\gamma-1)}}$$

This equation yields values of equal to 567.9 and 1313 for the hot jet and cold jet cases, respectively. These values are higher than those predicted by the CFD solution by approximately 8%. The most likely reason for these higher flux values is that the isentropic relations assume uniform inviscid one-dimensional flow. In reality the flow is viscous and a boundary layer develops, causing the effective throat area to become smaller, thereby lowering the total mass flow rate for the same total pressure and temperature. Also, since the throat is curved, the sonic line will be curved and should increase the effective throat area. However, it is believed that this curvature effect is relatively small in relation to the boundary layer effect.

4.3 Time-Accurate Trajectory Prediction Solutions

To determine the dynamic effects of a missile staging maneuver, two dynamic simulations were executed. The only difference between the two simulations was the temperature of the jet. The free-stream conditions and the jet chamber conditions matched those used in the steady-state baseline simulations and are given in Tables 2 and 3 respectively. To ensure that any differences between the static and dynamic simulations are purely from the dynamic motion, the simulations use the same meshes and flow solver.

4.3.1 Initial Condition Solution

The first step in the dynamic simulation technique is to provide an initial condition. The initial conditions for the dynamic solutions are jet off and an initial gap/D of 0.0050. Ideally, the gap/D should be zero, but in order to maintain mesh communications between the outer flow-field and the interstitial region a small gap was necessary. As was discussed in Section 3.2.1 the interstitial region was initialized after the outer flow-field had been computed to relative convergence. The initial condition solution was then run until the computed axial-force coefficients had converged to four significant digits. These force coefficients are given in Table 6.

In order to check the validity of the initial condition solution an inviscid axisymmetric solution has been computed for the interceptor vehicle. The codes used were the time marching Aungier code [15] and the space marching Kutler code [16]. The results of the inviscid solution are compared to the initial condition solution in Figures 10 and 11. Figure 10 illustrates the bow shock location computed by the inviscid codes overlaid upon constant Mach number contours of the viscous initial condition solution. It is apparent that the bow shock has the correct shape. The initial condition solution does have a bow shock which appears to be slightly upstream and farther away from the body than the inviscid solution. This is expected as the initial condition solution is viscous. The boundary layer present in the initial condition solution causes the body

Table 6: Initial Condition Axial-Force Coefficients.

Gap/D	Booster	Interceptor
0.0050	1.764	0.076

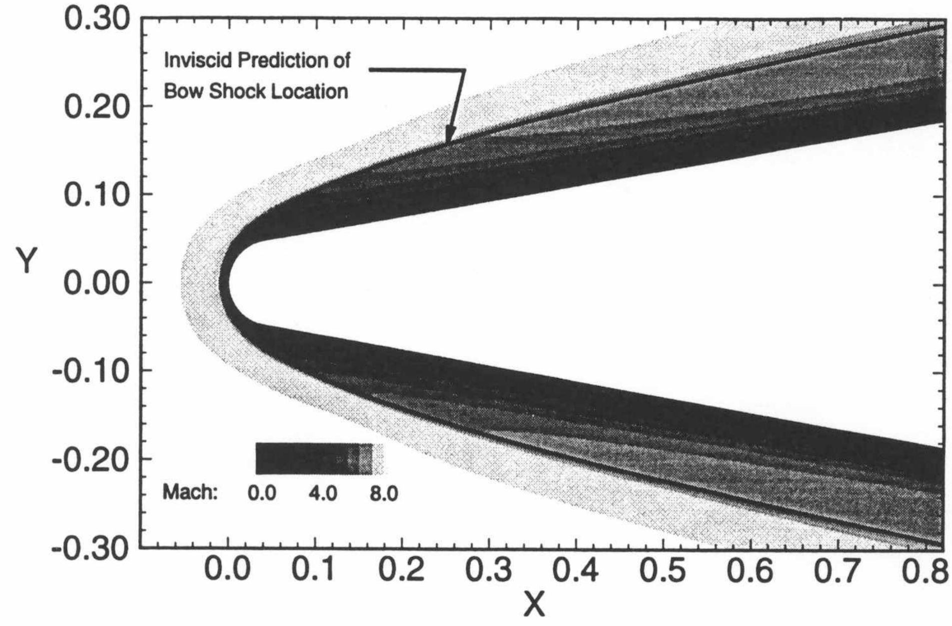

Figure 10: Interceptor Vehicle Bow Shock Location

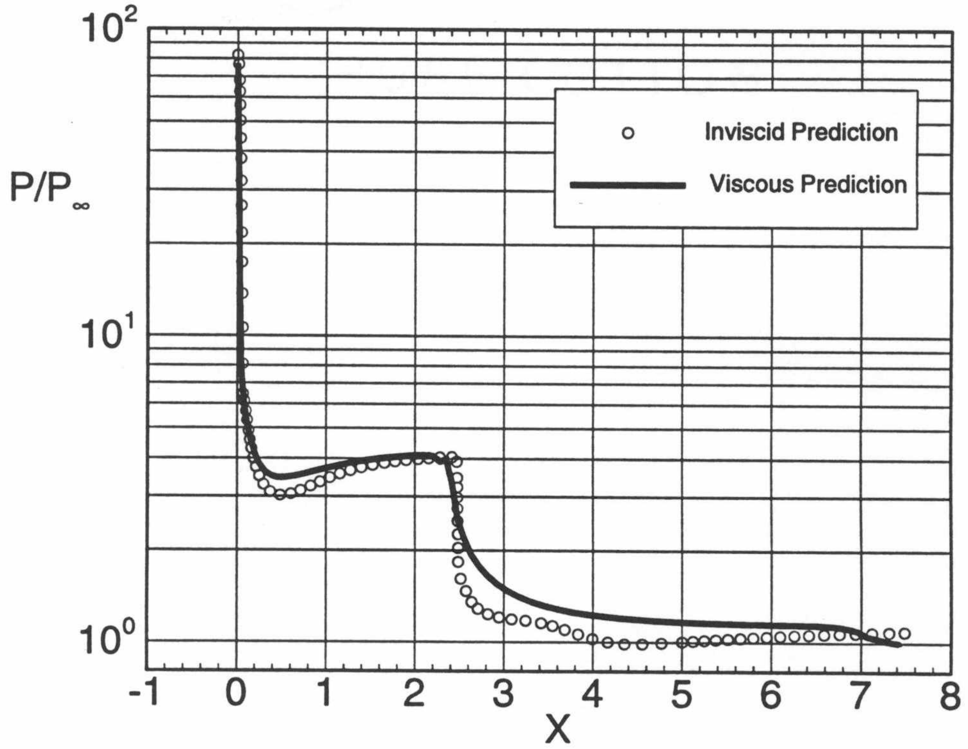

Figure 11: Interceptor Vehicle Surface Normalized Pressure Distribution

to be effectively larger and therefore displaces the bow shock slightly farther away from the body.

Figure 11 is another comparison of the inviscid solution and the initial condition solution. In this figure the non-dimensional surface pressure (P/P_∞) distribution is plotted against it's x location for the length of the interceptor vehicle. The symbols represent the inviscid solution and the line represents the initial condition solution. The agreement between the two solutions is good.

Another check that can be made is the isentropic stagnation conditions. Assuming that the shock on the stagnation line is approximately a normal shock, we can use the Rayleigh pitot formula:

$$\frac{P_{t2}}{P_1} = \left[\frac{(\gamma+1)M_1^2}{2}\right]^{\frac{\gamma}{\gamma-1}} \left[\frac{\gamma+1}{2\gamma M_1^2-(\gamma-1)}\right]^{\frac{1}{\gamma-1}}$$

Substituting the free-stream Mach number for M1 yields the following result:

$$\frac{P_{t2}}{P_1} = 81.0$$

As can be seen in Figure 11 the normalized pressure at the stagnation point is very close to that given by the Rayleigh pitot formula. The exact value from the initial condition solution is 77.1. This underpredicts the Rayleigh pitot value by approximately 5%. The reason for this underpredicition is most likely the fact that the bow shock has been smeared by the inclusion of artificial viscosity in the CFD solution.

4.3.2 Trajectory Predictions

For the prediction of the interceptor and booster trajectories, the flow solver was run with a timestep of 1.0×10^{-7} seconds per iteration. This small timestep was necessary to maintain numerical stability and resulted in a maximum CFL number on the order of 10 for the entire solution domain. Instead of moving the meshes every time step, the flow solver was run 100 steps per cycle and the meshes were moved at the end of the cycle. This was done to improve the efficiency of the computational process by staying in the flow solver longer during each cycle. The flow solver computed each mesh velocity based on dx / (100 * dt) for each timestep of the cycle. By running 100 steps per cycle the assumption was made that the mesh velocity over the cycle is constant. This assumption appears valid based on the very small time increments used and the smooth velocity history curves produced.

Both the interceptor vehicle and the booster were modeled with a mass of 141.1 lbm. The base area of both vehicles, 1.157 ft^2, was used to non-dimensionalize the axial forces. The simulations were run until t=0.050 seconds at which time the gap/D passed 0.25 for both the hot and cold jet cases. The time histories of the trajectory for these simulations are shown in Figures 12-15. In these figures the lines with the solid symbols indicate the hot jet simulation while the lines with the open symbols indicate the cold jet simulation. The lines with the square symbols are the booster values while the lines with the circular symbols are the interceptor vehicle values.

Figure 12 illustrates the time history of the axial-force coefficient. For both the hot jet and cold jet cases the trend is for the force to build to a peak and then decay to a steady force. Since the separation rocket motor is started from a no flow condition, it takes a finite amount of time for the jet to become fully developed. Once the jet has developed and the vehicles are separating, the force decays until it reaches an almost steady-state value. The hot jet case reaches a maximum force of 1.5 times the cold jet case, and reaches it's peak force coefficient earlier.

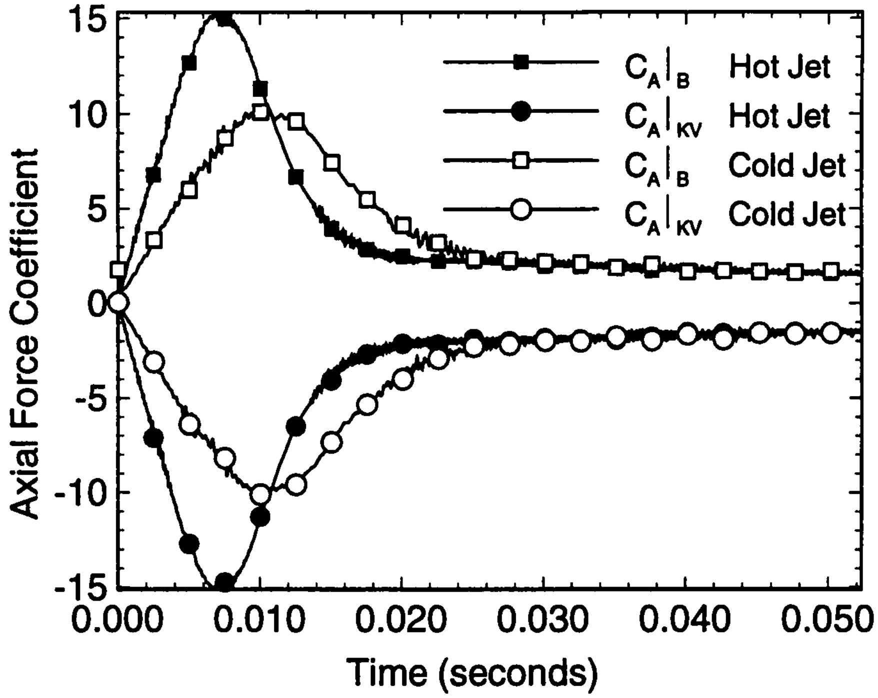

Figure 12: Axial-Force Coefficient versus Time.

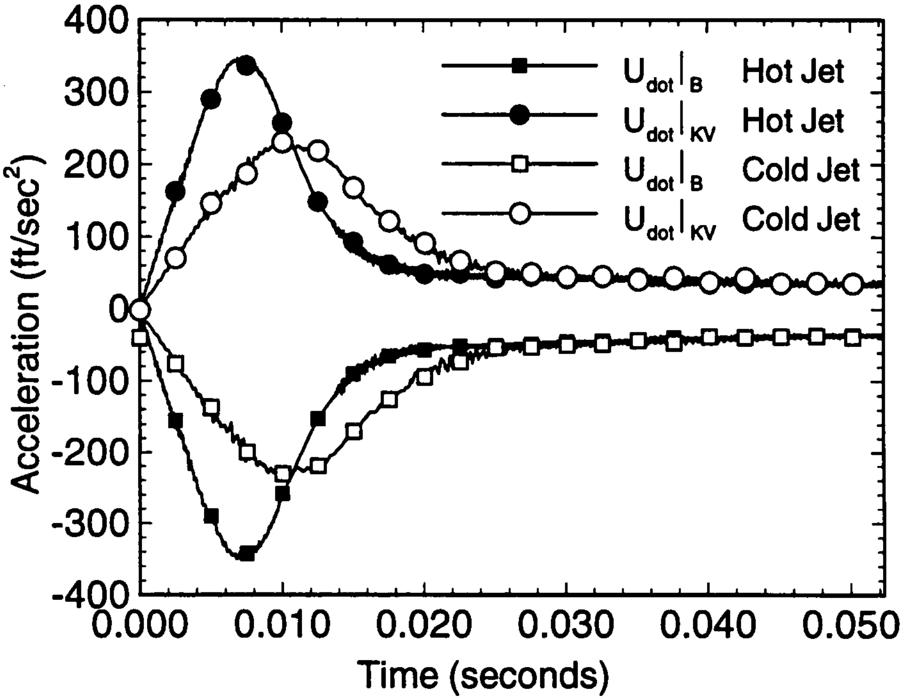

Figure 13: Axial Translation Acceleration versus Time.

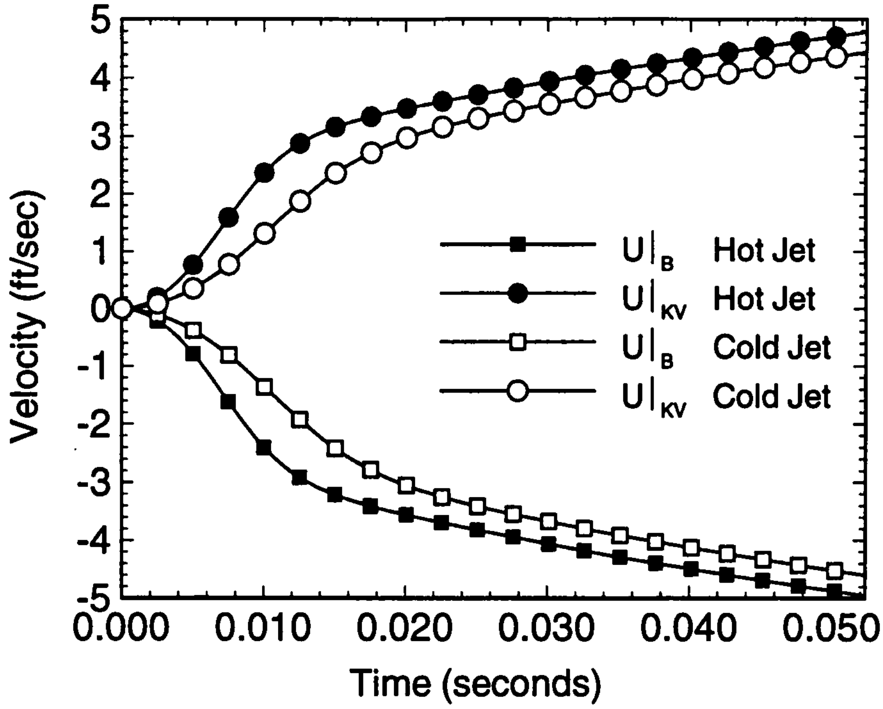

Figure 14: Axial Translation Velocity versus Time.

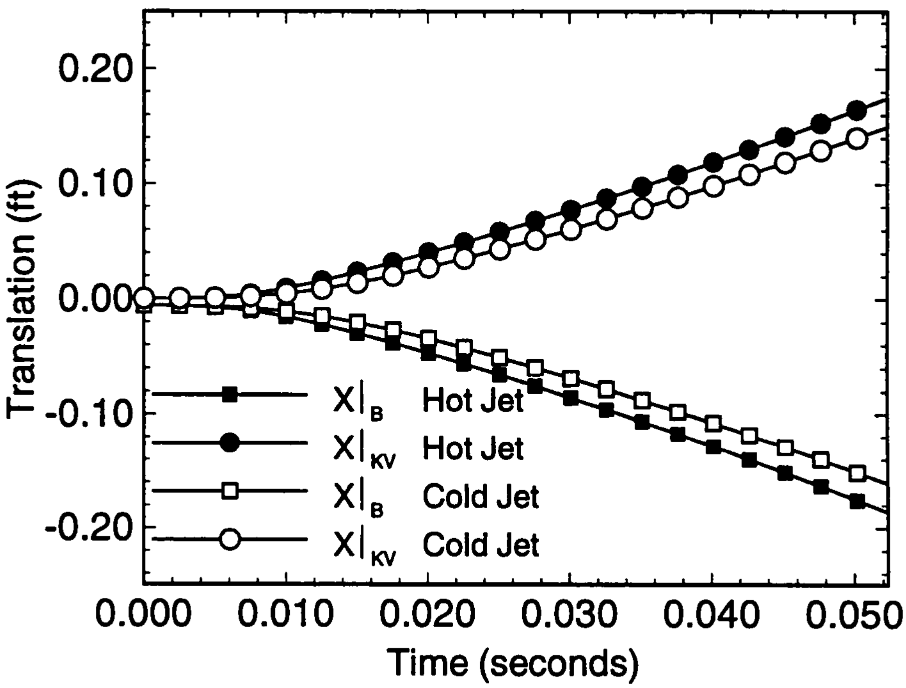

Figure 15: Axial Translation Distance versus Time.

The hot jet case peaks faster because the speed of sound in the hot jet is higher and thus flow phenomena propagate faster. Since the pressure builds faster in the hot jet case, the bodies do not have time to separate as much and therefore a higher peak pressure is observed. After approximately t=0.03 seconds, the differences between the hot jet and cold jet cases is almost negligible. This is similar to the observations that were made for the static cases.

It is interesting to note that there appears to be high frequency noise in these coefficients at distinct points on the curves. Most noticeable is in the time frame of 0.015-0.025 seconds on the hot jet curves. In order to examine this phenomena, an animation was produced of the interstitial region during this time frame. It was observed that the jet shear layer was oscillating. Whether this is a physical or numerical phenomena can not be explained here. The flow is probably turbulent in this region and no attempt was made to model turbulent flow in this study. These oscillations are an area for further study since substantial vibration could damage instruments or controls on the vehicles.

Figure 13 shows the time history of body acceleration. Note that the peak acceleration for the hot jet and cold jet cases are approximately 10 and 8 times the acceleration of earth's gravity. Also note the magnitude of the oscillations described in the paragraph above imply a force approximately equal to the force of gravity acting on the bodies at very high frequencies.

Figure 14 is an illustration of the time history of the velocity of the bodies. As expected, the hot jet case reaches a higher velocity earlier, but later in the simulation the velocity difference between the hot jet case and the cold jet case becomes constant. This is expected as the difference in forces becomes negligible as was seen in Figure 12.

Figure 15 shows the history of translation distance versus time. Here, it can be seen that at 0.050 seconds, the vehicles in the hot jet case have separated approximately 0.05 feet farther than in the cold jet case.

Shown in Figures 16,and 17 are the axial-force coefficient versus gap/D and the gap/D versus time respectively for the hot jet and cold jet cases. Figure 16 shows that the peak

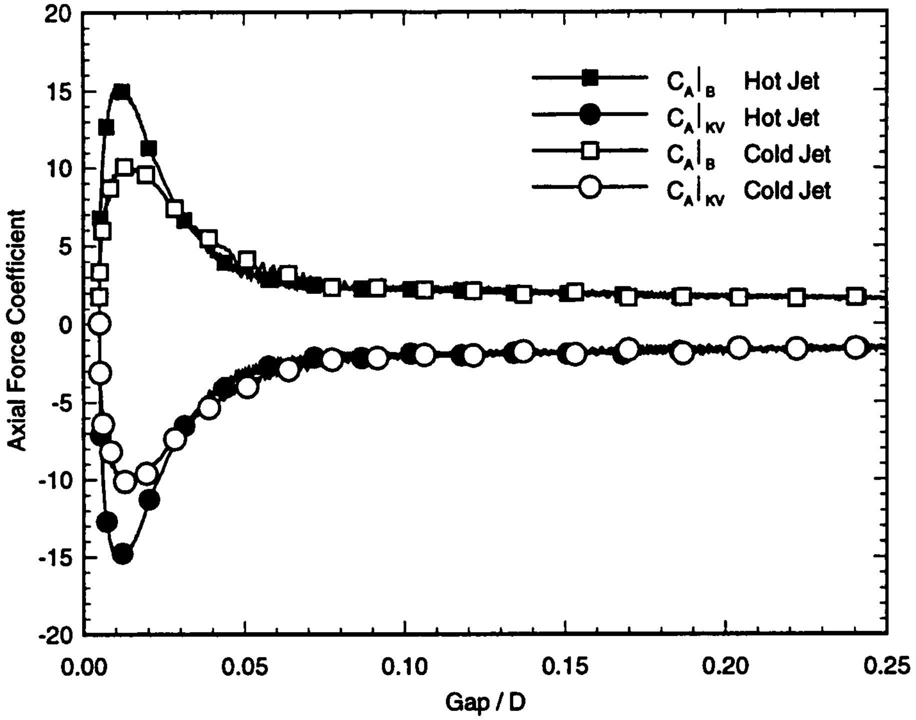

Figure 16: Axial-Force Coefficient versus Gap/D.

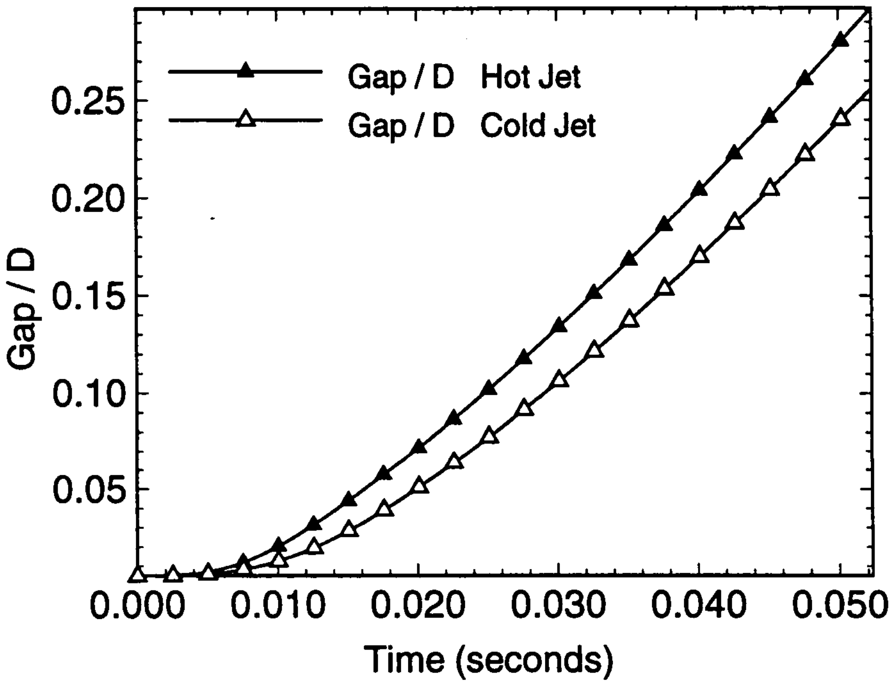

Figure 17: Gap/D versus Time for Hot Jet and Cold Jet Time-Accurate Simulations.

forces for each case occur at approximately the same gap/D. Figure 17 illustrates the difference between the hot jet and cold jet cases.

Figure 18 is a comparison of the dynamic and static axial-force coefficients versus gap/D. The symbols represent the static values and the lines are the dynamic values. It is evident that the dynamic cases are much different from the static cases in the gap/D range of 0.0 < gap/D < 0.04. For a value of gap/D >= 0.25 the dynamic loads are identical to the static loads; and hence there are no dynamic effects happening at this separation distance with respect to the axial-force coefficient. The most obvious point about this graph is the large difference between static and dynamic axial-force coefficients developed at gap/D=0.0075. The loads of the static cases are more than twice that developed for the dynamic cases at the same gap/D. This can be explained by the fact that the jet for the dynamic case was started from zero flow, and did not fully develop, before the bodies had separated more than 0.0075 gap/D. It is also interesting to note that at a gap/D of 0.0170, the hot jet and cold jet static cases are almost identical while the hot jet and cold jet dynamic cases have significant differences. Again, this is attributable to the development time of the jet and the fact that the hot jet develops faster than the cold jet because the speed of sound is directly proportional to the gas temperature. The reason that the dynamic solutions overshoot the forces of the static solutions at gap/D=0.0170 is also a dynamic effect. The interstitial region probably has a fluid dynamic nature different from its steady-state value at the same gap/D. That is, motor startup effects have not had time to reach steady-state.

An animation has been produced to illustrate the time-accurate dynamic solution. Selected frames from that animation are presented in Figure 19. As was the convention in the earlier static simulation figures, the top half of each frame shows the hot jet simulation and the bottom half of each frame shows the cold jet simulation. The frames in the left column indicate Mach number contours and the frames in the right column illustrate normalized temperature contours. The timestep between each frame is 0.005 seconds. Recall that for the steady-state

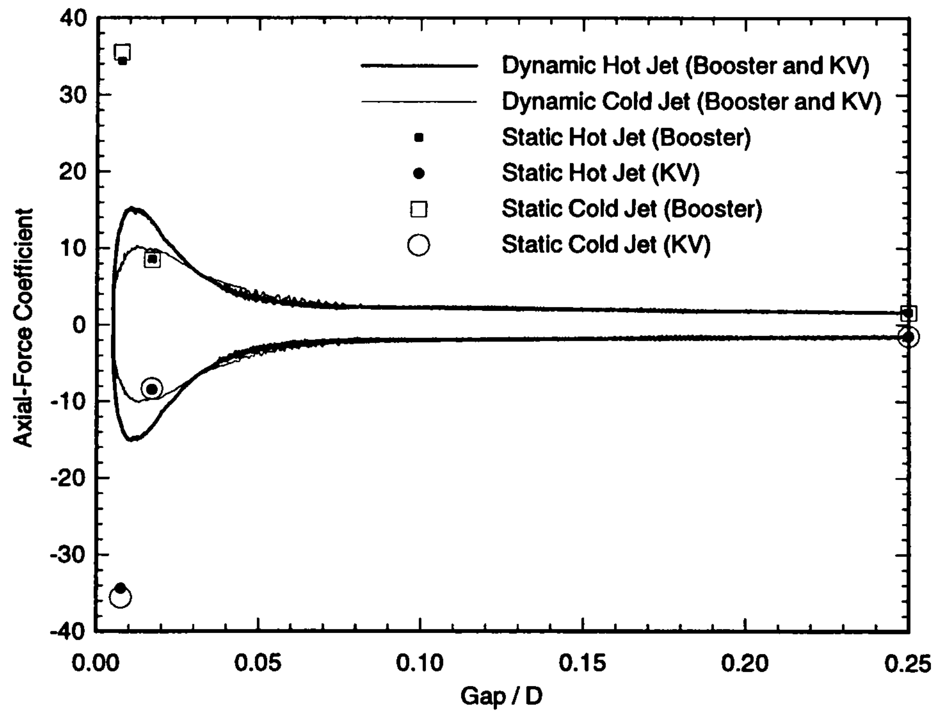

Figure 18: Axial-Force Coefficient versus Gap/D for Steady-State and Time-Accurate Simulations.

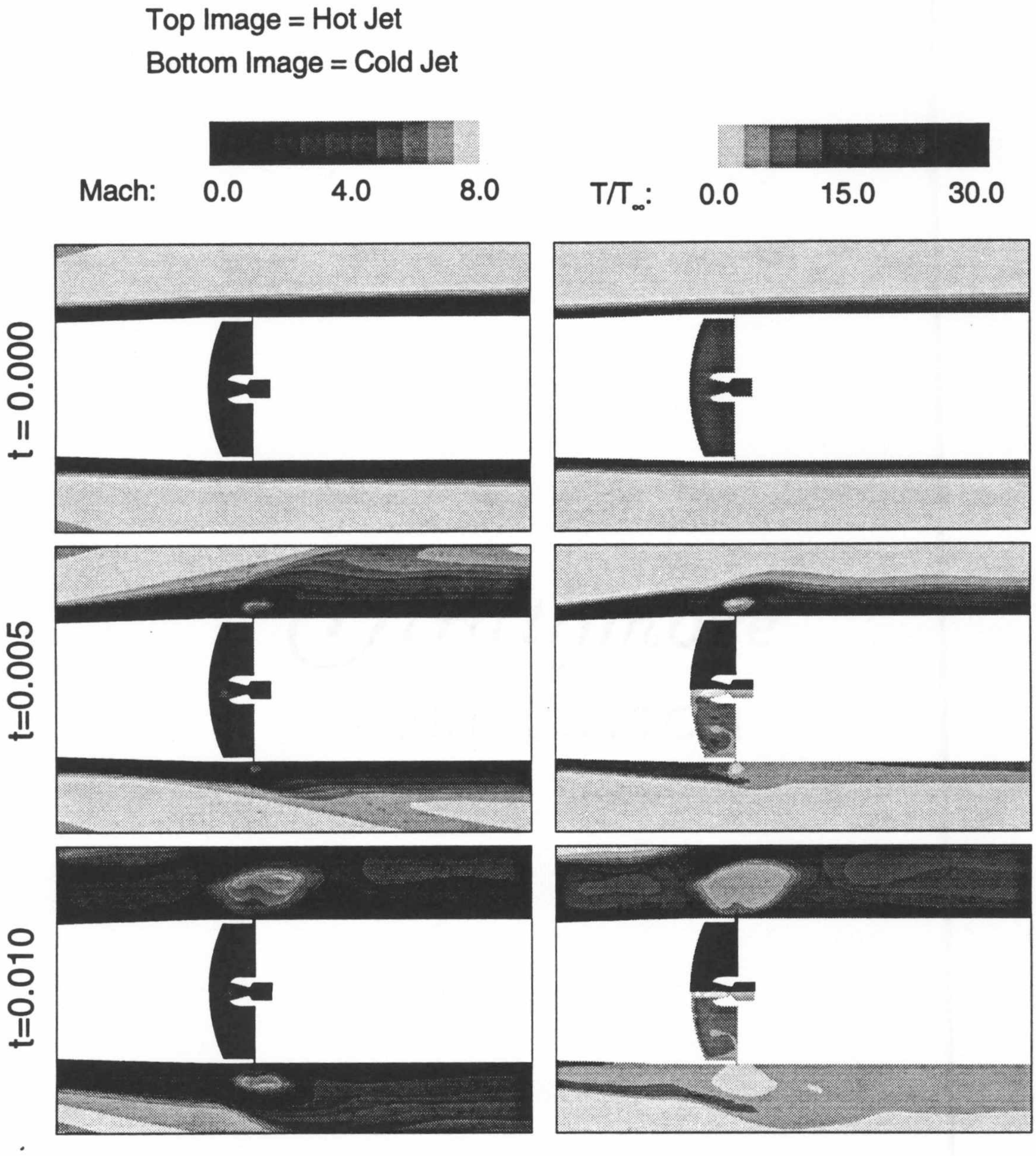

Figure 19: Time-Accurate Staging Results (animation frames)

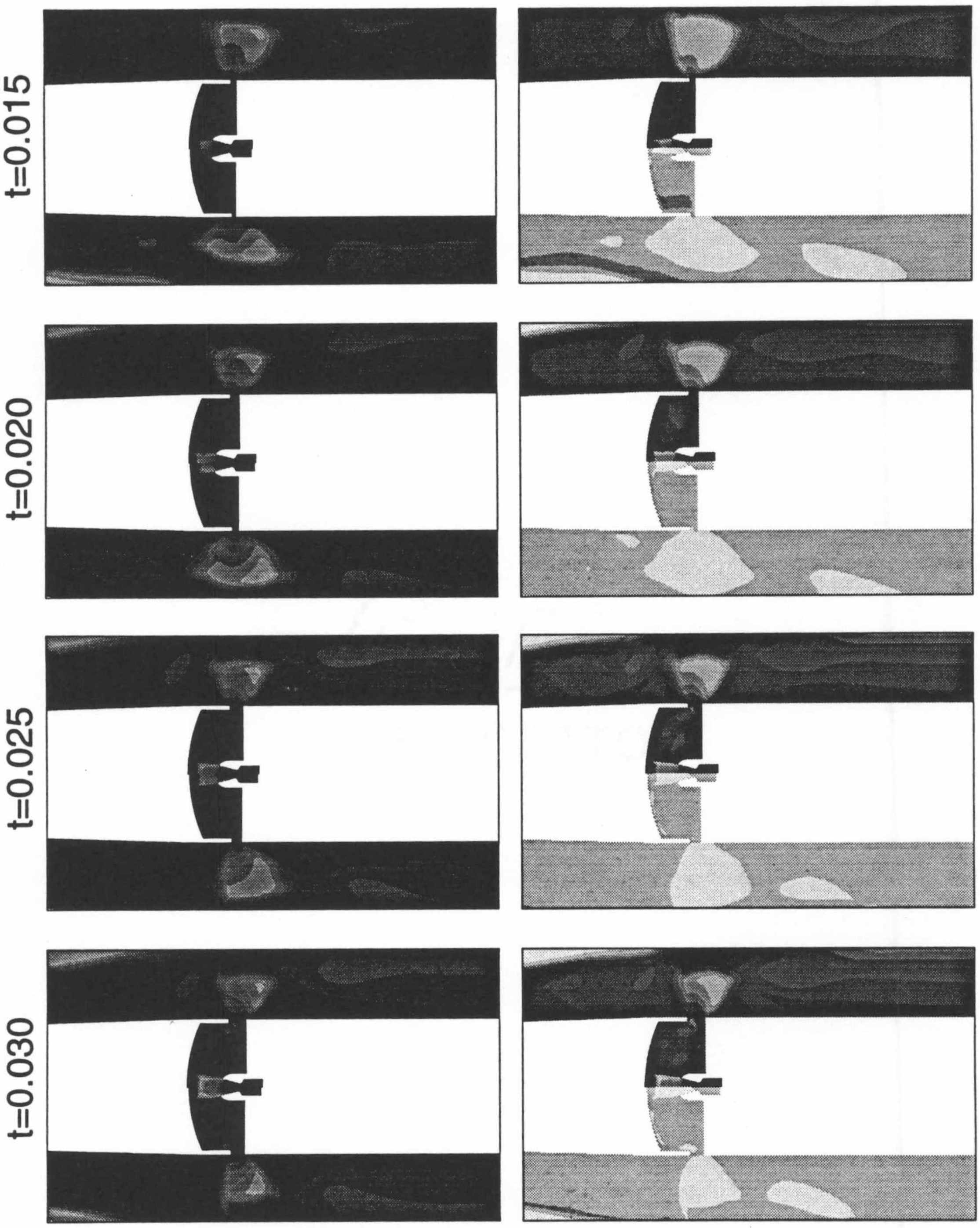

Figure 19 (continued).

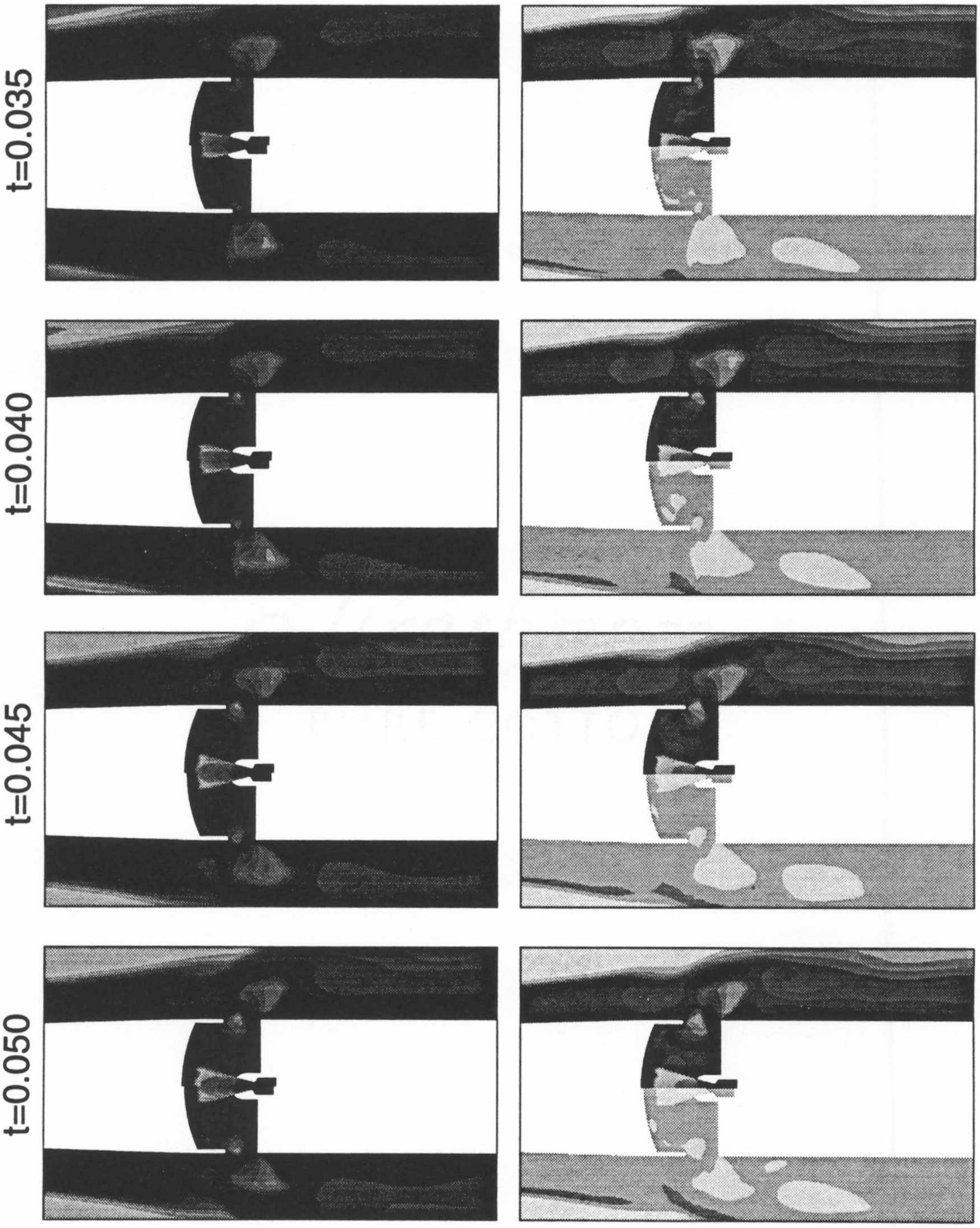

Figure 19 (continued).

baseline cases, (Figs 6-9) the Mach number contours were almost identical when comparing the hot jet cases and cold jet cases. In Figure 19 the differences between the Mach contours for a given time slice is due to the differences in the separation rocket motor flow development in the interstitial region. After t=0.03 the Mach number contours again look similar for both the hot and cold jet cases.

Chapter 5

CONCLUSIONS AND RECOMMENDATIONS

Based on the results and analysis conducted for this study, several conclusions can been reached and some recommendations for future work can be given. Testing to obtain axial forces of an axisymmetric missile staging event, within a facility like the AEDC VKF, is valid for gap/D > 0.1. The use of a cold jet is valid to obtain axial forces in static cases. If high temperature gases affecting control or instrumentation systems is a concern, then a hot jet simulation is required even for static tests. Static modeling should not be done for cases where the gap/D is less than 0.1, since significant dynamic effects are encountered in this region, primarily caused by separation rocket motor start-up. Also, the cold jet assumption is not valid when gap/D < 0.1.

It is recommended to use an integrated test and evaluation approach. Time-accurate CFD should be used for the closest gap/D with the appropriate jet temperature and motor start-up transients, and wind tunnel testing should be used for gap/D > 0.1. The CFD solution would then provide a good initial condition for subsequent wind tunnel static simulations and trajectory calculations. This approach would utilize the merits of both CFD and wind tunnel testing to their best advantage.

Future computational work in the missile staging area would be to include turbulence modeling and real gas effects to determine their effects on the staging process. An investigation of the high frequency force oscillations should be conducted to determine if this is a physical or numerical effect. Vibrations could be detrimental to the instrumentation or controls of the flight vehicles. Ultimately, a three dimensional simulation should be performed to determine the effects that would be encountered should the vehicles become misaligned axially or if the staging maneuver occurred while the vehicles are at an angle of attack with respect to the free-stream flow.

BIBLIOGRAPHY

BIBLIOGRAPHY

[1] Billingsley, J.P., Burt, R.H., and Best, J.T. "Store Separation Testing Techniques at the Arnold Engineering Development Center. Volume III, Description and Validation of Captive Trajectory Store Separation Testing in the Von Kármán Facility." AEDC-TR-79-1, March 1979.

[2] Hall, L.H., and Mitchell, C.R. "An Unsteady Multi-Body Analysis Technique for Missile Staging Events Using Enriched Structured Grids." Proceedings of the First AFOSR Conference on Dynamic Motion CFD, June 1996.

[3] Dougherty, F.C., Benek, J.A., and Steger, J.L. "On Applications of Chimera Grid Scheme to Store Separation." NASA-TM-88193, October 1985.

[4] Benek, J.A., Steger, F.C., Dougherty, F.C., and Buning, P.G. "Chimera: A Grid Embedding Technique." AEDC-TR-85-64 (AD-A167466), December 1985.

[5] Dougherty, F.C. and Kuan, J. "Transonic Store Separation Using a Three-Dimensional Chimera Grid Scheme." AIAA Paper No. 89-0637, January 1989.

[6] Benek, J.A., Steger, J.L., and Dougherty, F.C. "A Flexible Grid Embedding Technique with Applications to Euler Equations." AIAA Paper No. 83-1944, July 1983.

[7] Benek, J.A., Buning, P.G., and Steger, J.L. "A 3-D Chimera Grid Embedding Technique." AIAA Paper No. 85-1523, July 1985.

[8] Thoms, R.D., and Jordan, J.K. "Investigation of Multiple-Body Trajectory Prediction Using Time-Accurate Computational Fluid Dynamics." AIAA Paper No. 95-1870, June 1995.

[9] Jordan, J.K., Suhs, N.E., Thoms, R.D., et. al. "Computational Time-Accurate Body Movement: Methodology, Validation, and Application." AEDC-TR-94-15, October 1995.

[10] Suhs, N.E., and Tramel, R.W. "PEGSUS 4.0 User's Manual." AEDC-TR-91-8 (AD-A280608), November 1991.

[11] Beam, R. and Warming, R.F. "An Implicit Factored Scheme for Compressible Navier-Stokes Equations." AIAA Paper No. 77-645, June 1977.

[12] Pulliam, T.H. and Steger, J.L. "On Implicit Finite Difference Simulations of Three-Dimensional Flows." AIAA Paper No. 78-10, January 1978.

[13] Benek, J.A., Donegan, T.L., and Suhs, N.E. "Extended Chimera Grid Embedding Scheme with Application to Viscous Flows." AIAA Paper No. 87-1126, July 1987.

[14] Dietz, W.E. "General Approach to Calculating Forces and Moments on Overset Grid Configurations." Proceedings of the Second Overset Grid and Solution Technology Symposium, October 1994.

[15] Aungier, R.H. "A Computational Method for Exact, Direct, and Unified Solutions for Axisymmetric Flow Over Blunt Bodies of Arbitrary Shape." AFWL-TR-70-16, July 1970.

[16] Kutler, P., Reinhardt, W.A., and Warming, R.F. "Multishocked, Three-Dimensional Supersonic Flowfields with Real Gas Effects." AIAA Journal, May 1973.

VITA

Richard Thoms was born in Knoxville, Tennessee on July 25, 1966. He graduated from West High School in June of 1984. While attending the Tennessee Technological University in Cookeville he also spent two years on co-op assignment with the Tennessee Valley Authority at the Sequoyah Nuclear Plant. He graduated with a Bachelor of Science in Mechanical Engineering from Tennessee Tech in December of 1989. The following February he started work for Calspan at the Arnold Engineering Development Center. His initial work assignment was as a Project Engineer for maintenance and repair projects. He soon started taking graduate courses at the University of Tennessee Space Institute to pursue a Master of Science Degree with a major in Mechanical Engineering. In October of 1993 he requested and received a transfer to the Computational Fluid Dynamics section. In this position he was able to work on the topic discussed in this thesis. His Master of Science degree was awarded in December of 1996. In October of 1996 he took a new position and is presently employed with CFD Research Corporation in Huntsville, Alabama.